Free Radical Biology and Medicine 211 (2024) 145–157

Contents lists available at ScienceDirect

Free Radical Biology and Medicine

journal homepage: www.elsevier.com/locate/freeradbiomed

Redox differences between rat neonatal and adult cardiomyocytes under hypoxia

Alexandra D. Ivanova [a,1], Daria A. Kotova [a,1], Yulia V. Khramova [b,a], Ksenia I. Morozova [b], Daria V. Serebryanaya [b], Zhanna V. Bochkova [b], Anastasia D. Sergeeva [a,b], Anastasiya S. Panova [a], Ivan A. Katrukha [b], Aleksandr A. Moshchenko [c], Vladimir A. Oleinikov [a,d], Alexey V. Semyanov [a,b,e,f], Vsevolod V. Belousov [c,a,g], Alexey G. Katrukha [b], Nadezda A. Brazhe [b,a,*], Dmitry S. Bilan [a,g,**]

[a] M.M. Shemyakin and Yu.A. Ovchinnikov Institute of Bioorganic Chemistry, Russian Academy of Sciences, Moscow, 117997, Russia
[b] Faculty of Biology, M.V. Lomonosov Moscow State University, Moscow, 119234, Russia
[c] Federal Center of Brain Research and Neurotechnologies, Federal Medical Biological Agency, Moscow, 117997, Russia
[d] National Research Nuclear University Moscow Engineering Physics Institute, Moscow, 115409, Russia
[e] Sechenov First Moscow State Medical University, Moscow, 119435, Russia
[f] College of Medicine, Jiaxing University, Jiaxing, Zhejiang Province, 314001, China
[g] Center for Precision Genome Editing and Genetic Technologies for Biomedicine, Pirogov Russian National Research Medical University, Moscow, 117997, Russia

ARTICLE INFO

Keywords:
Cardiomyocytes
Hypoxia
Hydrogen peroxide
Genetically encoded fluorescent biosensor
Raman microspectroscopy

ABSTRACT

It is generally accepted that oxidative stress plays a key role in the development of ischemia-reperfusion injury in ischemic heart disease. However, the mechanisms how reactive oxygen species trigger cellular damage are not fully understood. Our study investigates redox state and highly reactive substances within neonatal and adult cardiomyocytes under hypoxia conditions. We have found that hypoxia induced an increase in H_2O_2 production in adult cardiomyocytes, while neonatal cardiomyocytes experienced a decrease in H_2O_2 levels. This finding correlates with our observation of the difference between the electron transport chain (ETC) properties and mitochondria amount in adult and neonatal cells. We demonstrated that in adult cardiomyocytes hypoxia caused the significant increase in the ETC loading with electrons compared to normoxia. On the contrary, in neonatal cardiomyocytes ETC loading with electrons was similar under both normoxic and hypoxic conditions that could be due to ETC non-functional state and the absence of the electrons transfer to O_2 under normoxia. In addition to the variations in H_2O_2 production, we also noted consistent pH dynamics under hypoxic conditions. Notably, the pH levels exhibited a similar decrease in both cell types, thus, acidosis is a more universal cellular response to hypoxia. We also demonstrated that the amount of mitochondria and the levels of cardiac isoforms of troponin I, troponin T, myoglobin and GAPDH were significantly higher in adult cardiomyocytes compared to neonatal ones. Remarkably, we found out that under hypoxia, the levels of cardiac isoforms of troponin T, myoglobin, and GAPDH were elevated in adult cardiomyocytes, while their level in neonatal cells remained unchanged. Obtained data contribute to the understanding of the mechanisms of neonatal cardiomyocytes' resistance to hypoxia and the ability to maintain the metabolic homeostasis in contrast to adult ones.

Abbreviations: ROS, reactive oxygen species; IRI, ischemia-reperfusion injury; ETC, electron transport chain; OGD/OGR, oxygen-glucose deprivation/restoration; OD, oxygen deprivation; NHE, Na^+/H^+ exchanger; RS, Raman spectroscopy.

* Corresponding author. Department of Biophysics, Biological Faculty, Moscow State University, 119234, Russia:
** Corresponding author. M.M. Shemyakin and Yu.A. Ovchinnikov Institute of Bioorganic Chemistry, Russian Academy of Sciences, Moscow, 117997, Russia.
E-mail addresses: nadezda.brazhe@biophys.msu.ru (N.A. Brazhe), d.s.bilan@gmail.com (D.S. Bilan).
[1] These authors contributed equally.

https://doi.org/10.1016/j.freeradbiomed.2023.11.034
Received 15 October 2023; Received in revised form 26 November 2023; Accepted 27 November 2023
Available online 1 December 2023

1. Introduction

The widespread prevalence of cardiovascular diseases poses complex challenges for modern science. According to the World Health Organization, ischemic heart disease ranks first among the causes of mortality in the population [1,2]. Currently, it is known that most cardiac pathologies, including hypertrophy, ischemia, heart failure, inflammation, and fibrosis are associated with disruptions in signaling pathways involving redox reactions [3–7]. Reactive oxygen species (ROS), comprising superoxide anion radicals, hydrogen peroxide, hydroxyl anions, peroxynitrite and hypochlorite anions play a pivotal role in these mechanisms [8,9]. Under typical physiological circumstances, cellular ROS levels are regulated by antioxidant systems encompassing superoxide dismutases, catalase, glutathione peroxidases, peroxiredoxins as well as glutathione- and thioredoxin-dependent systems, among others [3,9–12]. In diverse cell types, including cardiomyocytes, controlled production of ROS plays a crucial role in preserving cellular balance by governing numerous signaling pathways. For example, hydrogen peroxide (H_2O_2) is an essential signaling molecule that participates in signal transduction pathways through the reversible modification of amino acid residues in proteins [13–15]. In cardiomyocytes, ROS regulate vital processes like differentiation, proliferation, and electromechanical coupling [16–18]. However, the disruption of the equilibrium between ROS production and activity of protective antioxidant systems leads to the emergence of oxidative stress. Consequently, elevated ROS concentrations induce cellular oxidation, resulting in damage to DNA, lipids, proteins, and other macromolecules.

It is generally accepted that oxidative stress occurs during myocardial infarction and subsequent reperfusion in the heart [19,20]. Reperfusion is necessary to rescue heart function during myocardial infarction, but the restoration of blood flow can also cause additional damage to the heart, known as ischemia-reperfusion injury (IRI). IRI is a significant risk factor contributing to the morbidity and mortality associated with cardiovascular disease [21–23]. Recently, significant efforts have been made to understand the origins of oxidative stress during ischemia/reperfusion and develop approaches for its correction.

The main sources of ROS formation in cardiomyocytes include the mitochondrial respiratory chain (electron transport chain, ETC), NADPH oxidases, xanthine oxidase, NADPH reductases, cytochrome P450, and monoamine oxidase [17,24,25]. Under ischemic conditions, ROS generation in cardiomyocytes is attributed to mitochondrial respiratory chain dysfunction [26], xanthine oxidase activation [27], and the oxidation of iron (Fe^{2+}) within the oxyhemoglobin complex [28]. Meanwhile, it is widely believed that a predominant surge in ROS production occurs during reperfusion, making a significant contribution to the development of oxidative stress [29].

Although the consequences of ROS effects on various cell types including cardiomyocytes might be critical for cell structure, physiology and metabolism, cells may react to oxidative stress through multiple adaptation mechanisms. Upregulation of expression of multiple proteins is one of the fundamental pathways that helps the cell to sustain survival and functionality in oxygen-deficient situations. For example, it has been previously demonstrated that the expression of such proteins as troponin T and myoglobin increased under hypoxic conditions providing the maintenance of contractile apparatus function and oxygen preservation in various types of cells [30–32].

Despite significant scientific interest in this field, the role of redox modifications and contributors to oxidative stress during pathological cardiac conditions remains one of the least explored areas. The revolution in redox biology began with the development of genetically encoded fluorescent sensors. These biosensors are now widely used in various biomedical and biological research studies. For instance, the HyPer biosensor is a powerful tool for monitoring H_2O_2 dynamics *in vivo* within tissues of transgenic organisms [33]. Genetically encoded fluorescent instruments from the HyPer family have become highly demanded in recent years in redox process studies, prompting a reevaluation of the role of H_2O_2 in various biological processes [34–37].

Various genetically encoded biosensors have been used to study heart tissues, with metabolic biosensors for registration of ATP [38], lactate, pyruvate [39], as well as cyclic nucleotides (cAMP, cGMP) [40–42]. In the present study we employed HyPer7 for H_2O_2 detection [43] and SypHer3s for monitoring pH dynamics [44].

Our study has a tripartite aim, with a strong emphasis on the investigation of redox-state and highly reactive substances within cardiac cells. Firstly, we seek to quantify and compare the generation of H_2O_2 and pH in neonatal and adult cardiac cells under hypoxic conditions. Secondly, our focus extends to examining the impact of hypoxia on the redox state of mitochondria in both adult and neonatal cardiomyocytes, applying Raman microspectroscopy to unravel how oxygen deprivation influences the redox state of c- and b-type cytochromes in ETC. By the estimation of the ETC redox state we analyzed the ETC loading with electrons that is closely coupled to the generation of the superoxide anion-radical ($O_2^{\bullet-}$) in complexes III. Lastly, we aim to investigate the dynamic of four pivotal cardiospecific proteins following hypoxia/reoxygenation, potentially uncovering adaptive mechanisms that counteract the detrimental effects of reactive oxygen species.

2. Materials and methods

2.1. Animal husbandry

SHR male rats (2-month-old, 180–210 g) were bred and housed in the animal facilities of the Institute of Bioorganic Chemistry of the Russian Academy of Sciences (IBCh RAS) in a 12 h light-dark cycle with free access to food and water. For neonatal cardiomyocyte cell culture, neonatal rat pups (1–3 days after the birth) were obtained from adult SHR rats. The work was accomplished under the supervision of the IBCh IACUC and following the Regulations of the Ministry of Health of the Russian Federation. All procedures were approved by IBCh IACUC protocol No 372 from March 13, 2023.

2.2. Isolation and culture of neonatal rat cardiomyocytes

Rat neonatal cardiomyocytes were obtained from the hearts of a single litter (7–13 pups) of SHR rats. All solutions used in the protocol were sterile-filtered, and all tools were sterilized with 70 % alcohol prior to the procedures. Except for the initial tissue extraction, all subsequent steps were performed within a sterile laminar flow environment. Initially, the rat pups were decapitated, and their hearts were extracted and placed in a cold PBS solution (137 mM NaCl, 2.7 mM KCl, 10 mM Na_2HPO_4, 1.8 mM KH_2PO_4, pH 7.4) on ice. The ventricles were then isolated from the atria and blood vessels, and the epicardium was removed. The isolated ventricles were minced and suspended in a solution containing a mixture of enzymes (Neonatal Heart Dissociation Kit, mouse and rat, Miltenyi Biotec), followed by incubation at 37 °C for 15 min. This resuspension and incubation process was repeated two more times, resulting in a total incubation time of 45 min for the enzymatic treatment. The tissue homogenate was subsequently transferred to a cell culture medium DMEM/F12 (BioloT), containing penicillin/streptomycin (1 %, PanEco), Fetal Bovine Serum (FBS, 10 %, BioloT) and filtered through a 70 μm cell strainer (SPL Life Sciences). The cells were then centrifuged for 5 min at 600 g, the supernatant was removed, and the cells were resuspended in 1 mL of PEB buffer (PBS, 10 % BSA, 2 mM EDTA). To eliminate erythrocytes, the cells were incubated for 1 min in a red blood cell lysis solution (Miltenyi Biotec). After another centrifugation step for 5 min at 600 g, the supernatant was removed. The cells were resuspended in 1 mL of DMEM/F12 with glutamine and counted using a Goryaev chamber. Following cell counting, the cells were plated in 35-mm plastic Tissue Culture Dishes (SPL Life Sciences) in 1 mL DMEM/F12, with a seeding density of 5x10^5 cells per dish. For transient expression of biosensors, we used AAV-based vectors with cloned HyPer7 or SypHer3s genes. Cells were infected with viral particles at a

MOI of 10 000 VG/cell. The fluorescence signal of the biosensors expressed in neonatal cardiomyocytes was measured on the 5-7th day after transduction under hypoxia/reoxygenation conditions.

2.3. Isolation and culture of adult rat cardiomyocytes

Isolation of adult rat cardiomyocytes was performed according to the described protocol [45] with little changes. All solutions used in the protocol were sterile-filtered, all tools and Langendorff perfusion system were sterilized with 70 % alcohol prior to the procedures. Except for the initial tissue extraction and enzymatic perfusion all subsequent steps were performed within a sterile laminar flow environment. Ten minutes prior to the procedure, the animal received an intraperitoneal injection of heparin (1000 units/kg). Subsequently, the rat was anesthetized with 5 % isoflurane and then decapitated. The chest was opened, and the heart was briefly excised and washed with a Krebs-Henseleit buffer (KHB) solution (118 mM NaCl, 4.8 mM KCl, 25 mM HEPES (PanEco), 1.25 mM $MgSO_4$, 1.25 mM K_2HPO_4, 11 mM D-glucose, 5 mM Taurine (Sigma), pH 7.4). The heart was then cannulated through the aorta for retrograde Langendorff perfusion using a KHB solution aerated with carbogen (95 % O_2, 5 % CO_2). After perfusing 100 mL of KHB solution and removing the blood, the perfusion was switched to an enzyme solution consisting of KHB with the addition of 1 g/L bovine serum albumin (BSA, PanEco), 0.6 g/L Collagenase Type II (Worthington Biochemical Corp.), 0.05 g/L Protease Type XIV (Sigma), and 25 μM $CaCl_2$. The enzyme solution was recirculated through the heart for 40–50 min. Subsequently, the heart was transferred to a sterile laminar flow box, the atria were removed, the ventricles were minced and suspended using a pipette with a trimmed tip in a Petri dish with 5 mL of KHB solution supplemented with 10 mM BDM (2,3-Butanedione monoxime). Next, 5 mL of KHB–B solution (consisting of KHB with the addition of 10 mM BDM, 10 g/L BSA, and 0.1 mM $CaCl_2$) was added, and the cell suspension was filtered through a 100 μm strainer. The strainer was additionally rinsed with 5 mL of KHB–B solution. The cell suspension was centrifuged at 100 g for 3 min. After removing the supernatant, the cells were suspended in 25 mL of KHB–B solution and gently mixed. The cells were allowed to settle under their own weight for a period of 5–7 min. Once again, the supernatant was removed, and the cells were resuspended in 25 mL of KHB–B solution. Calcium was gradually introduced to the solution by titrating 20 mM $CaCl_2$, adding 250 μl, 375 μl, and 500 μl at intervals of 3–5 min. Following this, the cell suspension underwent another round of centrifugation at 100*g* for 3 min. The supernatant was removed, and the cells were suspended in 5 mL of culture medium containing DMEM high glucose (4.5 g/L), 1 % penicillin/streptomycin (1 %, PanEco), 2 mM glutamine (Gibco), and 10 % FBS (BioloT). The cells were then plated on laminin-coated confocal dishes (SPL Life Sciences), with an excess of approximately 300–500 μl per dish. Over the next 3 h, any non-adherent cells were removed. The medium volume in the dish was adjusted to 2 mL. On the following day after isolating the cardiomyocytes, viral particle transduction was performed. Fluorescence visualization was carried out on the 5th day after cell isolation.

2.4. Genetic constructs and viruses

The genetic constructs cTnT-HyPer7-mito and cTnT-SypHer3s-cyto were introduced using adeno-associated viruses (AAVs) of serotype PHP.S and serotype 9 (AAV-PHP.S for HyPer7 and AAV9 for SypHer3s). To achieve precise expression of these constructs in cardiomyocytes, a cardiac-specific promoter was employed. This promoter is a constitutive hybrid promoter composed of the CMV immediate early enhancer fused to the cardiac troponin T promoter (cTnT). The cTnT promoter was inserted into the multiple cloning site (MCS) of the AAV9 plasmid (Stratagene) using *Mlu*I and *Eco*RI (FD, ThermoFisher Scientific) restriction sites. The genes encoding the biosensors HyPer7 [43] and SypHer3s [44] were then inserted into the MCS of the AAV9-cTnT vector using *Eco*RI and *Hind*III (FD, ThermoFisher Scientific) restriction sites. In order to localize the biosensor HyPer7 in the mitochondrial matrix, the respective gene was equipped with a duplicated mitochondrial targeting sequence (MTS2) [46]. The SypHer3s-cyto constructs, which did not contain any subcellular localization signals, were employed for biosensor expression in the cytosol. The virus titers were 4.8*10^12 VG/mL for AAV9-cTnT-SypHer3s-cyto and 8.1*10^12 VG/mL for AAV-PHP.S-cTnT-HyPer7-mito.

2.5. Dynamics of H_2O_2 and pH in neonatal and adult cardiomyocyte cell culture under oxygen-glucose deprivation/restoration conditions

Imaging of H_2O_2 and pH dynamics in neonatal and adult cardiomyocyte cell cultures was performed using an Olympus Fluoview FV3000 inverted fluorescent microscope equipped with a gas mini-incubator (Miniature Incubator TC-MWP, Bioscience Tools), where 35 mm glass coverslips with cardiomyocytes had been placed. For HyPer7 and SypHer3s DAPI/FITC/Cy3/Cy5 Quad smb LED Set filters were used for excitation (λ_{ex} = 370–420 nm and λ_{ex} = 447–503 nm) and for emission (λ_{em} = 495–527 nm). All the measurements were carried out using an Olympus UPLFLN 20× Objective.

Half an hour prior to the experiment, the cell medium in the dishes was replaced with a control Tyrode solution for fluorescence microscopy. To simulate oxygen-glucose deprivation/restoration (OGD/OGR) conditions, a custom-designed perfusion setup was used, that allows to switch the perfusion flow from normal oxygenated Tyrode solution (118 MM NaCl, 4.7 MM KCl, 2.2 MM NaH_2PO_4, 1.2 MM $MgCl_2$, 1.2 MM $CaCl_2$, 25 MM $NaHCO_3$, pH 7.2–7.4) to deoxygenated Tyrode solution. Control Tyrode solution contained 5 mM glucose, while the deoxygenated solution was free of glucose to induce OGD conditions. The detailed description of the perfusion setup was previously reported at [47].

The control and deoxygenated perfusion solutions were prepared by saturating the Tyrode solution in 1-L tanks with air, CO_2, or N_2 using a gas controller (CO_2–O_2-MI, Bioscience Tools). For the control solution, a gas mixture of 5 % CO_2 and 95 % air was bubbled into the tank, for the hypoxia solution, a gas mixture of 5 % CO_2 and 95 % N_2 was used. The oxygen concentration was continuously monitored using fluorescent oxygen sensors (FTC-PSt3) in the solution tanks and within the tubes of the perfusion system, both immediately before and after the flow into the dish. To capture the signal from the fluorescent oxygen sensors, optical fibers were connected to a multichannel oximeter (Multi-Channel Oxygen Meter OXY-4 SMA (G3)). The acquired signal was recorded using PreSens Measurement Studio 2 software. All components of the oxygen sensor system were obtained from PreSens Precision Sensing GmbH. To exclude oxygen leakage to the dish, N_2 was supplied to the mini-incubator, displacing O_2 from the external medium around the dish during hypoxia conditions, during normal/reoxygenation conditions, the mini-incubator was supplied with air. This setup allowed an exceptionally rapid (within 30–60 s), precise, and controlled alteration of the oxygen concentration in the cell medium. The oxygen concentration was changed from $pO_2 \sim 150$ mmHg (~20 % of the oxygen concentration in the air) to $pO_2 < 5$ mmHg (<1 % of the oxygen concentration in the air).

The protocol of the experiment was as follows. Each experiment involved the recording of the biosensor's signal for 10–15 min under normal conditions to establish the baseline fluorescent signal (perfusion with normal Tyrode solution with glucose). Then, the signal was recorded during OGD for 35 min (perfusion with deoxygenated Tyrode solution without glucose). Subsequently, the signal was recorded during OGR for 15 min (perfusion with normal Tyrode solution with glucose). After OGR, the perfusion was terminated, and H_2O_2 (200 μM) or L-lactate (20 mM) was added to the dish to elicit the maximal ratiometric response of the biosensors and validate live cells with an appropriate biosensor response.

2.6. Detection of cardiac troponin I, T and myoglobin by sandwich-type fluorescent immunoassay (FIA)

The concentrations of troponin I, troponin T and myoglobin in the cell lysates were determined by a sandwich-type FIA using monoclonal antibody pairs 19C7-560-Eu^{3+} (determining the concentration of cardiac troponin I), 329-406-Eu^{3+} (determining the concentration of cardiac troponin T) and 4E2-7C3-Eu^{3+} (determining the concentration of cardiac myoglobin) as described by Katrukha et al. [48] (all monoclonal antibodies were kindly provided by HyTest). For FIA, the capture antibodies (20 μg/mL, 0.1 mL/well in PBS) were sorbed onto the surface of the wells of a 96-well polystyrene plate by shaking for 30 min at RT. The wells were then washed with 10 mM Tris-HCl, 150 mM NaCl, 0.025 % Tween 20 and 0.05 % NaN_3 pH 7.8 (buffer A). After that, 0.025 mL of the sample was diluted in the stabilizing buffer (20 mM Tris-HCl buffer, 5 mM $CaCl_2$, 150 mM KCl, 7.5 % bovine serum albumin, 0.15 % NaN_3 pH 7.5) for troponin concentrations measurements or in the assay buffer (50 mM Tris-HCl buffer, 0.9 % NaCl, 0.01 % Tween 40, 0.5 % bovine serum albumin, 0.05 % NaN_3 pH 7.7) for myoglobin concentration measurements. After that 0.05 mL of detector antibodies (4 μg/mL) conjugated with a stable europium chelate (Eu^{3+}) were added into each well. The plates were incubated for 30 min at RT with constant shaking. After washing with buffer A, 0.2 mL of fluorescent enhancement solution was added to the wells of the plate, and then the fluorescence was detected using Victor X plate analyzer (PerkinElmer).

2.7. Cell lysates preparation

To prepare cell lysates, neonatal and adult cardiomyocytes were washed 3 times with PBS followed by the addition of 300 μl of lysis buffer (PBS with 0.1 % Triton X-100, 20 μg/mL phenylmethylsulfonyl fluoride, 3 μg/mL aprotinin, 1 μm pepstatin A). Then, the samples were subjected to ultrasonic treatment using Branson 450 Digital Sonifier (Branson), frozen and stored at −20 °C. The protein concentration in cell lysates was determined using the Bradford protein assay as described in Ref. [49]. The obtained values were utilized to normalize the troponins, myoglobin and GAPDH concentrations.

2.8. Western blot analysis

To assess the relative content of GAPDH, Western blot analysis with chemiluminescence detection was employed. Different quantities of chicken GAPDH that was used as a standard and protein samples from cardiomyocyte lysates were separated via 12.5 % SDS-PAGE and blotted onto 0.45 μM nitrocellulose membranes (Bio-Rad) according to the Towbin protocol [50]. Then immunostaining by anti-GAPDH mAbs (clone 4G5, HyTest), conjugated with horseradish peroxidase (HRP) was performed. GAPDH was visualized using SuperSignal West Femto Maximum Sensitivity Substrate (Thermo Scientific) on the ChemiDoc Touch Imaging System (Bio-Rad). Image quantification was performed using ImageLab 5.2.1 software (Bio-Rad). The total protein content in the cell lysates was normalized to β-actin content. The GAPDH content in the lysates of cardiomyocytes was calculated using a calibration curve showing band intensity of standard GAPDH samples versus their protein content.

2.9. Monitoring of the redox state of mitochondria in cardiomyocytes with Raman microspectroscopy

2.9.1. Recording of cardiomyocyte Raman spectra

To estimate the redox state of the respiratory chain of mitochondria in cardiomyocytes we used Raman microspectroscopy. Raman spectra of cultured adult or neonatal cardiomyocytes were recorded with confocal Raman microspectrometer InVia Qontor (Renishaw) with laser excitation wavelength 532 nm. Cells were grown on glass-bottom Petri dishes in a cell culture medium as described in sections 2.2 and 2.3. The cell culture medium was exchanged to the control Tyrode solution 30 min before the experiments. For the measurements Petri dishes were placed on the scanning table of the up-right Leica FSM microscope (Free-space-microscope) connected to the Raman microspectrometer and the water-immersion objective 63×, NA 0.9 (Leica) was used for the laser light focusing and the Raman scattering collection. The laser power was less than 0.5 mW for the registration spot with the diameter of 400 nm. Raman spectra were recorded from the central part of cardiomyocytes with the accumulation time of 60 s. Measurements of cardiomyocyte Raman spectra under normoxia (control conditions) were done under the perfusion of the Petri dishes with cardiomyocytes with the physiological solution continuously gassed 90 % O_2. The perfusion rate was 2–3 mL/min. Hypoxia (oxygen deprivation condition) was induced by the switching to the perfusion of cardiomyocytes with non-oxygenated physiological solution containing sodium dithionite (Sigma, 1 mg/ml). Sodium dithionite is known to be a highly efficient reducing agent that interacts with molecules in all phases of the sample and reduces O_2 and all oxidized molecules including ETC components, cytosolic hemoproteins, etc.

2.9.2. Analysis of Raman spectra

Raman spectra were analyzed with open-source software Pyraman, available at https://github.com/abrazhe/pyraman. The baseline was subtracted in each Raman spectrum and it was defined as a cubic spline interpolation of a set of knots, number and x-coordinates of which were selected manually outside any informative peaks in the spectra. The number and x coordinates of the knots were fixed for all spectra in the study, y coordinates of the knots were defined separately for each spectrum as 5 point neighborhood averages of spectrum intensities around the user-specified x-position of the knot. To choose the parameters for baseline subtraction we processed approximately 10 spectra from different cardiomyocytes. After the baseline subtraction, the intensities of peaks with the following maximum positions were defined: 570, 640, 750, 1126, 1365, 1370 and 1445-1450 cm^{-1}. Peak at 570 cm^{-1} corresponds to vibrations of cytochrome *c* heme in ruffled conformation with the decreased ability to accept and to donate electrons [51]; peak at 640 cm^{-1} is attributed to the vibration of C–S bond in *c*-type cytochromes (bond between Cys residue and heme *c*), Fe–S clusters and in non-oxidized Cys-containing proteins [52]. Peaks at 750 and 1126 cm^{-1} corresponds to bonds' vibrations in hemes of *c*-and *b*-type cytochromes [53–56]; peaks at 1365 and 1370 cm^{-1} – to deoxymyoglobin and oxymyoglobin [53–55], respectively, and peak at 1445-1450 cm^{-1} - to C–C bond vibration in lipids [53–56]. Though all listed cytochrome peaks are typical for Raman spectra of both redox cytochrome forms, it is known that in cells and tissues only reduced cytochromes are seen in Raman spectra due to their 100–1000 times higher Raman scattering intensity than that of oxidized cytochromes [56–59]. To estimate the redox state of cytochromes, conformation of cytochrome *c* heme, relative amount of C–S bonds and oxy-and deoxymyoglobin we used the following ratios of Raman peaks/intensities.

- I_{750}/I_{1450} and I_{1126}/I_{1450} ratios - as an estimation of the relative amount of reduced *c*-type and *b*-type cytochromes, respectively, normalized on the amount of lipids;
- I_{750}/I_{1126} - relative amount of reduced *c*-type cytochromes vs reduced *b*-type cytochromes;
- I_{570}/I_{750} - the probability of ruffled heme conformation in reduced cytochrome *c*;
- I_{640}/I_{750} - relative amount of proteins with non-oxidized Cys-residues or with Fe–S clusters;
- I_{1370}/I_{1450} - relative amount of oxymyoglobin vs lipids. Under normoxia conditions all myoglobin molecules are oxygenated, therefore this ratio corresponds to the total amount of myoglobin under control conditions;
- I_{1365}/I_{1450} - relative amount of deoxymyoglobin vs lipids. Under hypoxia all myoglobin molecules are deoxygenated, therefore this

ratio corresponds to the total amount of myoglobin under conditions of oxygen deprivation.

3. Results

3.1. H_2O_2 and pH dynamics in neonatal and adult cardiomyocytes cell culture under acute oxygen-glucose deprivation/restoration conditions

As oxidative stress plays a principal role in cardiovascular disease development, this study focuses on investigating the dynamics of hydrogen peroxide and pH. To track the real-time dynamics of the studied parameters at the level of individual cellular compartments, we used genetically encoded fluorescent biosensors. Specifically, we conducted visualization within the cytosol and mitochondrial matrix of cardiomyocytes. For monitoring the H_2O_2 dynamics, we employed the highly sensitive biosensor HyPer7 [43] localized in the mitochondrial matrix. The choice of localization was determined by our previous experiments, revealing that H_2O_2 generated in the cytosol rapidly diffuses into the mitochondrial matrix, while the reverse diffusion is limited [43]. Hence, when HyPer7 is localized in the mitochondria, it detects the general H_2O_2 pool regardless of the source of the oxidant. pH dynamics were visualized using the SypHer3s biosensor [44] in the cytosol. Meanwhile, to investigate the impact of OGD/OGR conditions on cardiomyocyte biochemical parameters, we utilized a setup that was previously established in our laboratory [47], which enables controlled and rapid modulation of oxygen levels in the perfusion chamber, alongside with the simultaneous microscopy of the studied subjects.

Using the highly sensitive H_2O_2 biosensor, HyPer7, we have found that redox events during hypoxia differ between neonatal and adult cardiomyocytes. Our experiments revealed that in neonatal

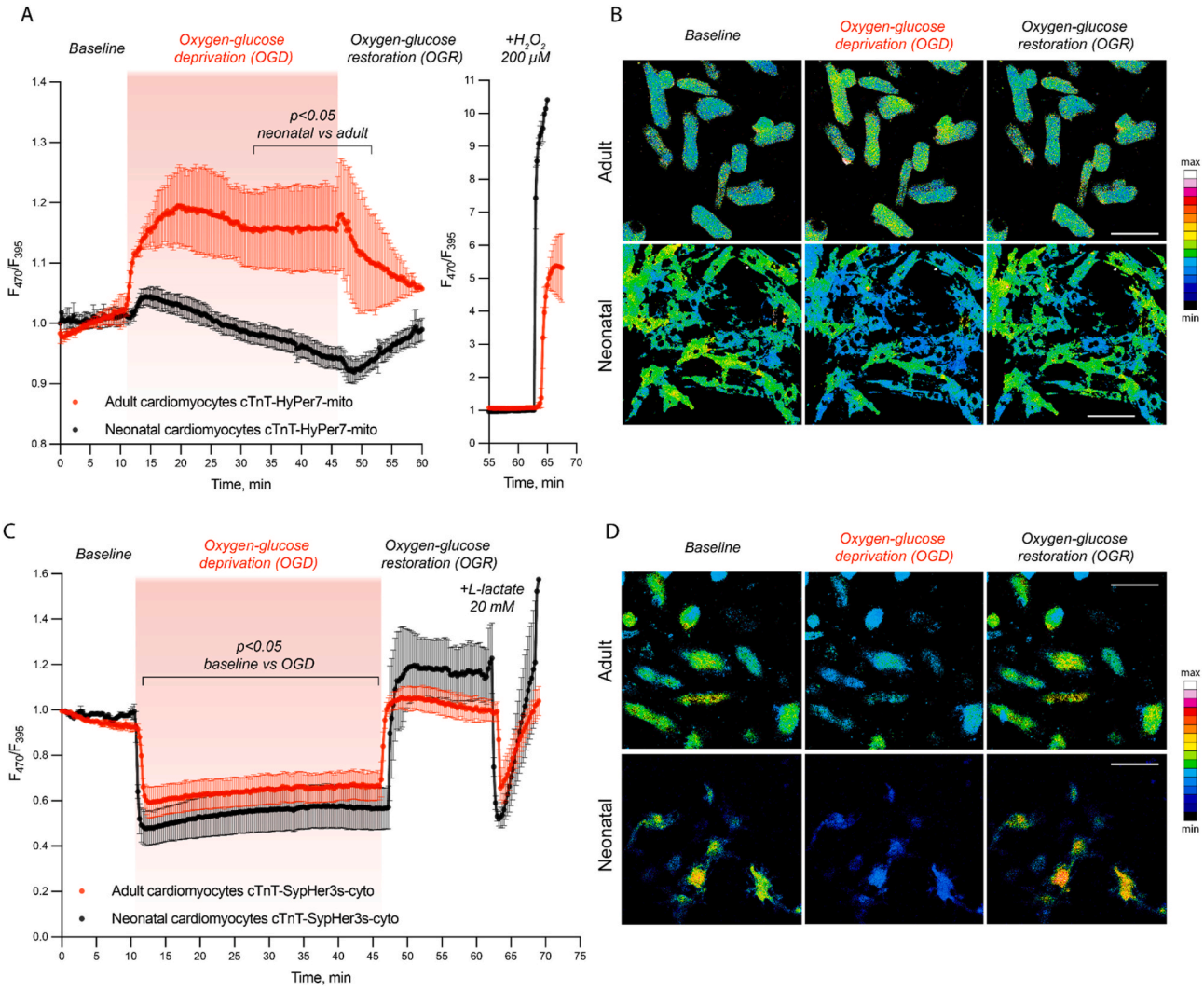

Fig. 1. Effects of OGD/OGR on H_2O_2 and pH in cultured neonatal and adult cardiomyocytes. A – real-time registration of H_2O_2 concentration using HyPer7 biosensor in the mitochondrial matrix of cultured neonatal (black) and adult (red) cardiomyocytes during 35 min of OGD and subsequent OGR. The graph represents the dynamics of a normalized HyPer7 signal (ratio F_{470}/F_{395} normalized to 1). Data averaged from 40 cells in 2 experiments for adult cardiomyocytes and from 86 cells in 3 experiments for neonatal cardiomyocytes. The HyPer7 signal response to the addition of 200 μM H_2O_2 is shown separately on the left. $P < 0.05$ - comparison of the HyPer7 signal from neonatal and adult cardiomyocytes, mixed-effects model, Šídák's multiple comparisons test. B - normalized HyPer7 ratio F_{470}/F_{395} in cultured adult (up) and neonatal (down) cardiomyocytes placed under OGD/OGR conditions (scale bar 100 μm). Sequentially shown: baseline, 35th minute of OGD and 15th minute of OGR. C - real-time registration of pH dynamics using SypHer3s biosensor in the cytosol of cultured neonatal and adult cardiomyocytes during 35 min of OGD and subsequent OGR. The graph represents the dynamics of a normalized SypHer3s signal (ratio F_{470}/F_{395} normalized to 1). Data averaged from 18 cells in 4 experiments for adult cardiomyocytes and 40 cells in 3 experiments for neonatal cardiomyocytes. The SypHer3s signal response to addition of 20 mM L-lactate shown on the graph. $P < 0.05$ - comparison of the SypHer3s signal between baseline and OGD/OGR, mixed-effects model, Šídák's multiple comparisons test. D – normalized SypHer3s ratio F_{470}/F_{395} in cultured adult (up) and neonatal (down) cardiomyocytes placed under OGD/OGR conditions (scale bar 100 μm). Sequentially shown: baseline, 35th minute of OGD and 15th minute of OGR. All data are presented as mean ± SEM.

cardiomyocytes, OGD induced a significant decrease in HyPer7 signal, registering 8.3 ± 1.5 % below baseline values at 35th minute of OGD, corresponding to reduced basal H_2O_2 concentrations under hypoxic conditions. During the OGR phase, we observed the restoration of the biosensor signal to its initial baseline values, indicating a resumption of H_2O_2 production (Fig. 1A). Notably, similar H_2O_2 dynamics were previously observed in neurons [47].

Conversely, within adult cardiomyocytes under OGD/OGR

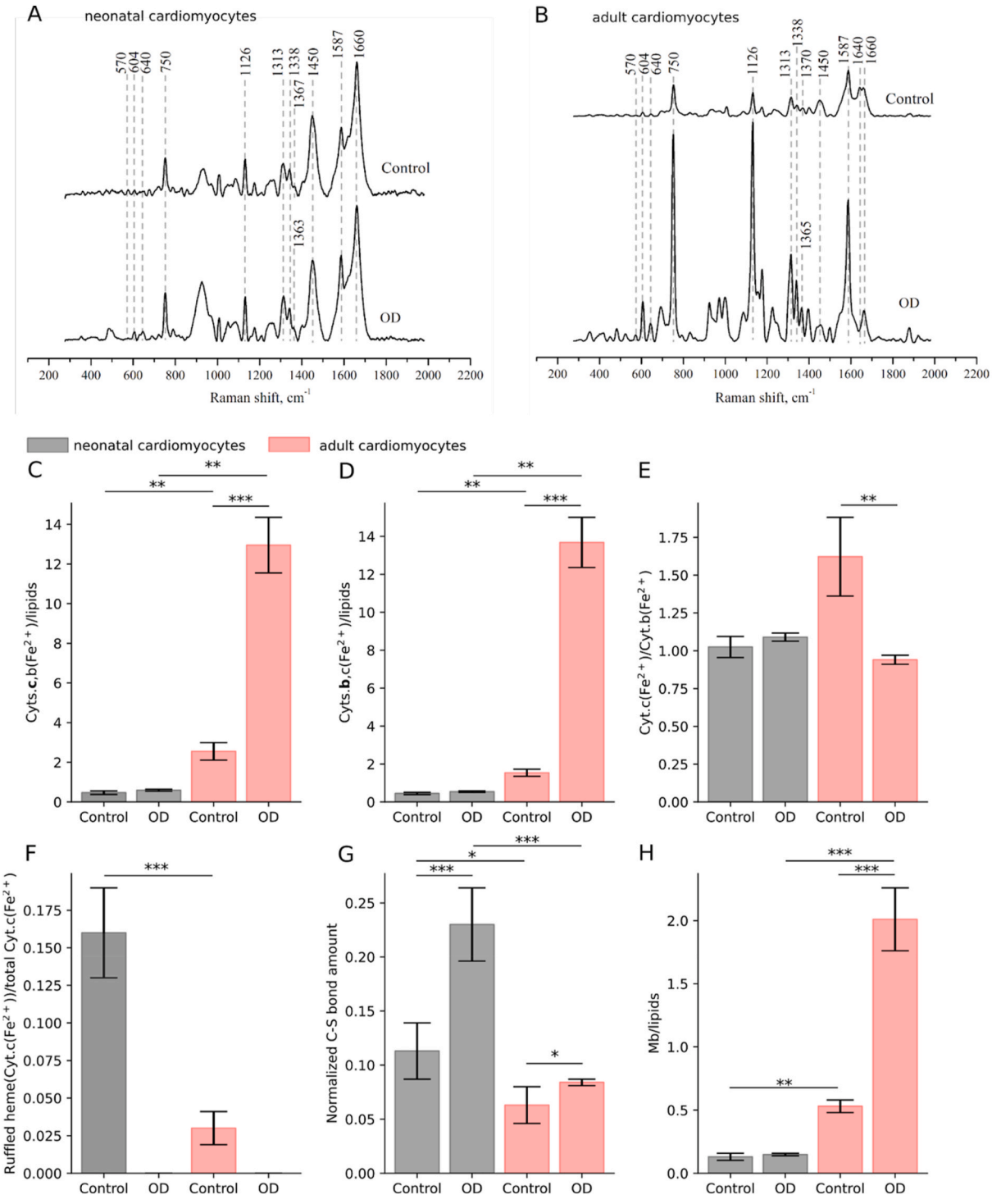

Fig. 2. Effect of oxygen deprivation on the redox state and relative amount of cytochromes in mitochondria of adult and neonatal cardiomyocytes. A, B - Raman spectra of neonatal and adult cardiomyocytes under normoxia (control, upper spectra) and oxygen deprivation (OD, lower spectra). For better representation spectra are shifted vertically and each spectrum is normalized on the intensity of its "lipid" peak with maximum at 1450 cm^{-1}. Numbers above peaks show the position of the peak maximum. C, D - relative amounts of reduced *c* and *b*-type mitochondrial cytochromes vs. lipids, respectively, in adult cardiomyocytes (red bars) and neonatal cardiomyocytes (grey bars) in control and oxygen deprivation conditions. E – relative amount of reduced *c*-type cytochromes vs. *b*-type cytochromes; F - relative amount of reduced cytochrome *c* with ruffled heme, possessing low ability to donate electron, normalized on the total amount of reduced cytochrome *c*; G - relative amount of C–S bonds in cytochrome *c* heme and molecules with reduced –SH groups normalized on the total amount of reduced *c*-type cytochromes; H - relative amount of myoglobin normalized on the amount of lipids. *, **, *** are p values < 0.05, 0.01 and 0.001, respectively (Mann-Whitney test).

conditions, H_2O_2 dynamics exhibited an inverse pattern compared to neonatal cardiomyocytes. In adult cardiomyocytes, the signal of the HyPer7 biosensor increased by 15.2 ± 6.9 % during OGD and gradually returned to its initial values during OGR. Substantial differences in biosensor values were observed between neonatal and adult cardiomyocytes from the 34th to 50th minutes of experiment (Fig. 1A). Both neonatal and adult cardiomyocytes exhibited a significant increase in the HyPer7 biosensor signal upon the introduction of H_2O_2 into the cellular environment, confirming its proper functionality (Fig. 1A).

Another detrimental factor for heart tissues during cardiac ischemia could be the accumulation of acidic metabolites, resulting in a reduction of both intracellular and extracellular pH, which could decrease to the values as low as 6.0–6.5 [60,61]. This tissue acidosis exacerbates ischemic damage and significantly impacts cardiac function. Thus, in the next step of this study, we examined the pH dynamics in both neonatal and adult cardiomyocytes under normal and hypoxia conditions using the genetically encoded fluorescent biosensor SypHer3s [44].

Upon exposure to OGD, a rapid onset of cytosolic acidosis was observed in both types of cardiomyocytes. The signal from the SypHer3s biosensor decreased by 41.7 ± 10.3 % and 29.2 ± 8.9 % in neonatal and adult cardiomyocytes, respectively (Fig. 1C). Remarkably, following OGR, the pH values in both neonatal and adult cardiomyocytes returned to their initial levels. According to the previously obtained data [47] this decrease in the normalized SypHer3s fluorescent signal equals approximately 0.5 pH units. At the end of each experiment series with both neonatal and adult cardiomyocytes, we introduced 20 mM lactate into the medium during imaging, observing the typical response of SypHer3s in these conditions: a sharp pH decrease followed by a rapid recovery to values higher than the initial ones. This phenomenon could be explained by the compensatory mechanisms of the cell. Thus, we have not observed significant differences in SypHer3s biosensor signal which reflects pH dynamics during OGD/OGR between neonatal and adult cardiomyocytes.

3.2. *Comparative study of hypoxia effect on mitochondria redox state in adult and neonatal cardiomyocytes*

Hypoxia is known to affect the redox state of the respiratory chain of mitochondria of many cell types including excitable cells [55]. Previously with resonance Raman spectroscopy (RS) it was demonstrated that hypoxia causes overloading of mitochondrial ETC in cardiomyocytes of isolated heart [54,55]. Here we applied RS with laser excitation at 532 nm to study the effect of oxygen deprivation on adult and neonatal cardiomyocytes. Expectedly, we observed the similar sets of peaks in Raman spectra recorded from these two types of cardiomyocytes (Fig. 2A and B). Thus, their Raman spectra demonstrated peaks corresponding to heme bond vibrations in reduced both *c*-and *b*-type cytochromes (peaks with maximum positions at 750, 1126, 1587 cm^{-1}), to reduced cytochrome *c* (570, 604, 1313 cm^{-1}), reduced *b*-type cytochromes (1338 cm^{-1}), C–C bond vibrations in lipids (1450 cm^{-1}) and C–N peptide bond vibration on proteins (1660 cm^{-1}) [53–56]. Besides, Raman spectra of cells demonstrated peaks of heme *b* vibration in oxymyoglobin (1367-1370 cm^{-1}) and deoxymyoglobin (1363-1365 cm^{-1}) [53–55]. We should also note that the peak at 750 cm^{-1} corresponds mainly to reduced cytochrome *c*, whereas the peak at 1126 cm^{-1} – to reduced *b*-types cytochromes [56–59]. Importantly, the peak at 570 cm^{-1} corresponds to bond vibrations in ruffled heme conformation in cytochrome *c* and by monitoring its relative intensity we can study changes in cytochrome *c* heme conformation and its ability to donate electron [51]. All spectra also demonstrated peak at 640 cm^{-1} that is a marker of C–S bonds in heme of *c*-type cytochromes, in non-oxidized thiol groups of Cys residues in proteins and Fe–S clusters [52].

We have found that the relative amount of reduced *c*-and *b*-type cytochromes in adult cardiomyocytes is much higher than in neonatal cardiomyocytes under both control and oxygen deprivation conditions (Fig. 2A–D). This difference is clearly seen from the Raman spectra (higher relative intensity of "cytochrome" Raman peaks in adult cardiomyocytes compared with neonatal cells) (Fig. 2A and B) and from histograms (Fig. 2C and D). Since hypoxic condition was caused by the application of sodium dithionite that reduces all available electron carriers exposing in Raman spectra all cytochrome-containing ETC complexes, we can conclude, that the total amount of ETC complexes and therefore the number of mitochondria in adult cardiomyocytes are significantly higher, than in neonatal cells. Moreover, in adult cells under normoxia conditions the percentage of ETC carriers with electrons is higher than in neonatal cardiomyocytes (Fig. 2C and D). Besides, under normoxia in adult cardiomyocytes the relative amount of reduced *c*-and *b*-type cytochromes vs. lipids is significantly lower (6–7 times), than under hypoxia. This result shows that under control conditions the ETC of adult cardiomyocytes is only partly loaded with electrons. This also means that hypoxia results in the accumulation of electrons in ETC including complex III, causing electron transfer to O_2 in the ubichquinone-binding site with the following superoxide anion-radical formation. To the contrary, the relative amount of reduced cytochromes in neonatal cardiomyocytes is almost the same under control normoxic and hypoxic conditions (Fig. 2C and D). It indicates that in neonatal cells under normoxia ETC is almost fully loaded with electrons and that hypoxia does not increase the amount of electrons in ETC and does not lead to excessed $O_2^{\bullet-}$ generation. These data can explain the observed decrease in H_2O_2 generation by neonatal cardiomyocytes under hypoxia compared to adult cardiomyocytes that respond to hypoxia by the increase in H_2O_2 amount (Fig. 1): in neonatal cells ETC seems to be in the non-functional state similar for both normoxia and hypoxia conditions, whereas in adult cells hypoxia results in the significant accumulation of electrons in ETC comparing to the normoxia state, thus enhancing $O_2^{\bullet-}$ generation in complexes III and I with the following formation of H_2O_2. Remarkably, we also observed differences in the redox state and heme conformation of cytochrome *c* in adult and neonatal cardiomyocytes. Cytochrome *c* in neonatal cells demonstrates higher probability of the ruffled heme conformation, than heme of cytochrome *c* in adult cells (Fig. 2F). Ruffled heme conformation is known for its low ability to transfer electrons [62,63]. This can be among reasons for the non-functional ETC state and similar full ETC loading with electrons in neonatal cells under normoxia and hypoxia conditions (Fig. 2C and D). In adult cardiomyocytes under normoxia the relative amount of reduced *c*-type cytochromes normalized on the amount of reduced *b*-type cytochromes is significantly higher, than under hypoxia or under both conditions in neonatal cells (Fig. 2E). We suggest that in adult cells under normoxia reduced cytochrome *c* molecules can accumulate in mitochondria intermembrane space if the complex IV does not reduce oxygen quickly enough. At the same time, the ratio between amounts of all molecules of *c*-and *b*-type cytochromes in mitochondria of adult and neonatal cardiomyocytes are similar as can be seen from Fig. 2E, oxygen deprivation (OD) conditions. We believe, that the observed increase in the ETC loading with electrons under hypoxia in adult cardiomyocytes is due to the lack of O_2 as of the terminal electron acceptor in the complex IV and not due to other factors as, for example, hypoxia-induced nitric oxide (NO) production. It is known that NO can interact with *a*-type cytochromes of the complex IV [64,65]. However, it was demonstrated that NO-induced inhibition of cytochrome *c*-oxidase occurred under high pO_2 values and not under hypoxia [64,65].

Expectedly, hypoxia in both cell types leads to an increase in the input of C–S bond Raman peak at 640 cm^{-1} to the spectra (Fig. 2A and B). Since this peak corresponds to C–S vibrations in reduced SH-groups, *c*-type cytochromes and Fe–S clusters, we performed normalization of the C–S bond Raman peak intensity on the intensity of cytochrome *c*-peak at 750 cm^{-1} to estimate hypoxia-induced changes in the relative amount of C–S bonds not in the reduced cytochrome *c*, but in non-oxidized Cys-residues and Fe–S clusters (Fig. 2G). We have found, that the relative number of molecules with such C–S bonds was higher in neonatal cardiomyocytes, than in adult cardiomyocytes under normoxia and hypoxia, and that hypoxia caused the increase in this parameter in

both cell types compared to the control condition (Fig. 2G). We attribute the observed differences between cells to the higher amount of glutathione and relative molecules in neonatal cardiomyocytes compared to adult cells. We also observed higher relative amounts of oxymyoglobin in adult cells, than in neonatal cardiomyocytes (Fig. 2H), that is due to the lower amount of myoglobin in neonatal cells. Hypoxia leads to the significant increase in the deoxymyoglobin amount in adult cardiomyocytes that can be explained by its de-novo synthesis under OD conditions (Fig. 2H). This result is in the agreement with the data obtained by independent measurements (Fig. 3B). Low amount of myoglobin in neonatal cells can be explained by the absence of necessity to store oxygen intracellularly, since these cells almost do not use oxidative phosphorylation and rely on glycolysis. These data are in agreement with our data that reveals the lower amount of ETC complexes in neonatal cells compared to adult cardiomyocytes (Fig. 2).

3.3. The effect of hypoxia on major cardiospecific protein content in neonatal and adult cardiomyocytes

Hypoxia is reported to alter the expression pattern of numerous structural and metabolic proteins in different cell types [66–69]. Biochemical profile variation appears to be one of the key mechanisms of promoting cell adaptability and maintaining cell survival in oxygen deficiency conditions. Herein, using FIA and Western blot analysis, we assessed the quantity of four important cardiac proteins: cardiac troponin I, cardiac troponin T, myoglobin, and GAPDH in normoxic and hypoxic conditions to examine how neonatal and adult cardiomyocytes respond to hypoxia in the context of protein expression (Fig. 3). First, under a normoxic state, we examined the content of the investigated proteins in neonatal and adult cardiomyocytes. Results of our experiments revealed that in normoxic conditions the content of all analyzed proteins was significantly higher in adult cardiomyocytes than in neonatal ones. The 20-, 10-,3- and 2-fold increase of cardiac troponin I (Fig. 3A), myoglobin (Fig. 2B), cardiac troponin T (Fig. 3C) and GAPDH content (Fig. 3D), respectively, was observed (Fig. 3A).

When considering hypoxic stress, we discovered that the biochemical profiles of neonatal and adult cardiomyocytes changed in response to OGD differently. It turned out that OGD has no effect on the relative content of all analyzed proteins in neonatal cardiomyocytes. However, in adult hypoxic cells the levels of cardiac troponin T, GAPDH and myoglobin were significantly (2-, 3- and 1,3- fold, $p < 0.05$, respectively) elevated compared to the control cardiomyocytes (Fig. 3B, C, D). In the case of troponin I level, no statistically significant difference between control and hypoxia-treated adult cardiomyocytes was observed (Fig. 3A).

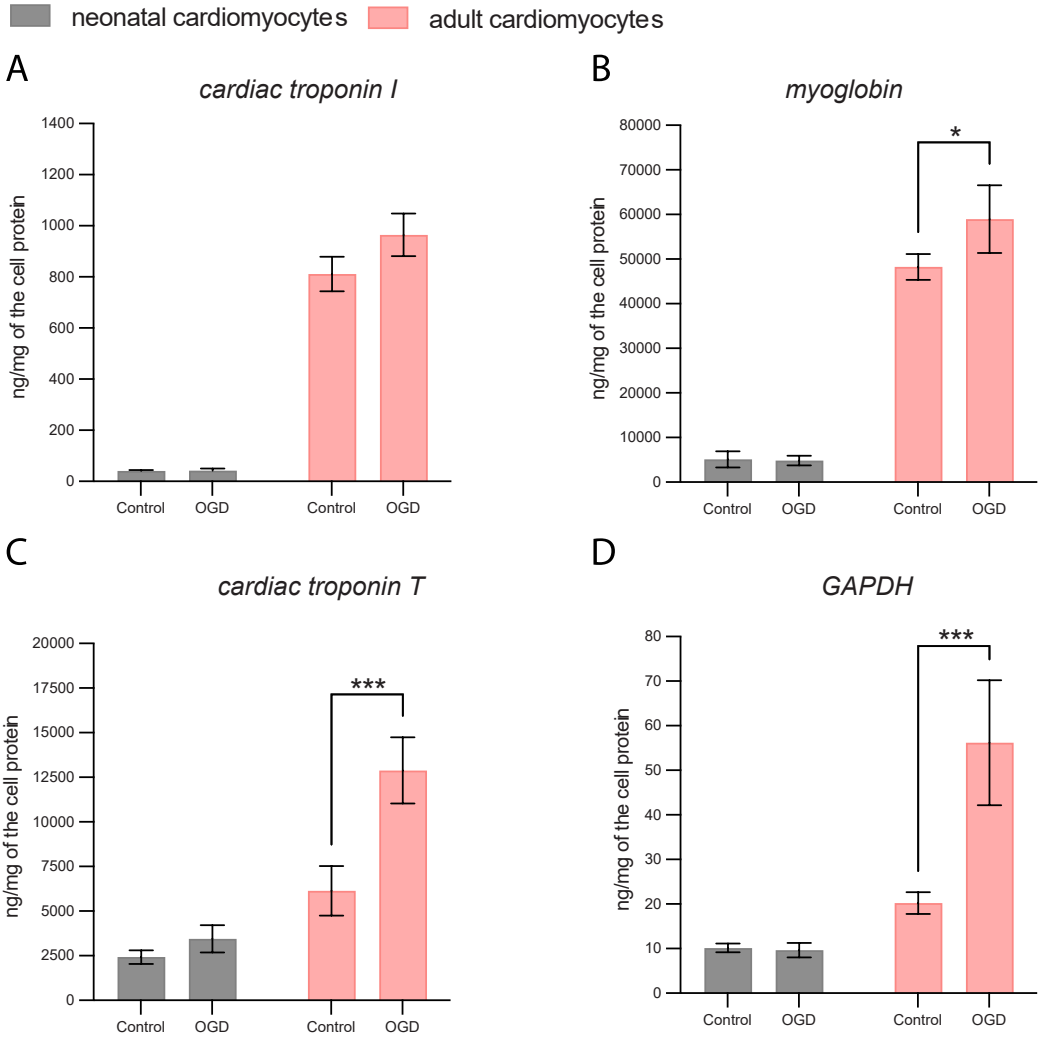

Fig. 3. The content of major cardiac proteins in control and OGD treated neonatal (grey bars) and adult (red bars) cardiomyocytes. A – cardiac troponin I, B – myoglobin, C – cardiac troponin T and D – GAPDH. * - $p < 0.05$, *** - $p < 0.001$, two-way ANOVA, Šídák's multiple comparisons test.

4. Discussion

Cardiovascular disease continues to be the leading cause of global illness and death. The myocardium's susceptibility to IRI is a significant vulnerability [23]. When oxygen availability is compromised in myocardial IRI, ROS are released, which can lead to the breakdown of mitochondria, disruption of energy production, and ultimately, the death of cardiomyocytes [70].

The metabolic response to acute myocardial ischemia is crucial for determining the fate of cardiomyocytes. In conditions of energy depletion, as observed in acute myocardial IRI, impaired mitochondria produce less ATP and generate more ROS, which are detrimental to cellular viability [71]. Recent insights into succinate accumulation during ischemia have revealed its role in triggering ROS generation upon reperfusion through reverse electron transport via mitochondrial complex I [25]. Notably, during ischemia/reperfusion, the activation of NADPH oxidases Nox2 and Nox4 also contributes to myocardial damage [72]. Controlled Nox2/4 activity is crucial for cardioprotective mechanisms, where ROS production regulates gene expression and provides myocardial protection [73].

Although there is extensive data suggesting the role of ROS in cardiomyocytes during ischemia-reperfusion, short-lived highly reactive compounds posed significant challenges. The utilization of genetically encoded fluorescent biosensors has helped mitigate these difficulties. These instruments are increasingly being used in cardiovascular disease models to visualize the redox regulation of specific cardiac conditions [74,75].

In addition to advancing novel technologies for investigating oxidative stress in the heart during ischemic scenarios, there is a necessity to explore different models. Isolated cardiomyocytes from adult animals or cultured cardiomyocytes from neonatal organisms are commonly used for this purpose. These cells are placed in specialized chambers that replicate hypoxia and reoxygenation conditions. Research focused on isolated cardiomyocytes is precise because it eliminates the potential influence of other cell types and circulating elements such as hormones, neurotransmitters, and cytokines [76]. This model is frequently used to study specific factors that cause cardiomyocyte damage during ischemia-reperfusion or cardioprotection [77,78]. Nevertheless, it is worth noting that findings derived from cell culture experiments may differ considerably from the actual dynamics occurring *in vivo*. Specifically, the pO_2 levels in cell cultures (approximately 140 mmHg in our study) are unachievable in living cardiac tissues, where this parameter seldom surpasses 90 mmHg [79]. Therefore, artifactual redox changes associated with the analysis of isolated biological samples is widely recognized [80].

Currently, there is no standardized protocol for inducing hypoxia-reoxygenation in cardiomyocyte cultures. While freshly isolated cardiomyocytes from adult animals yield the most representative results, neonatal cardiomyocyte cultures are increasingly utilized due to their ease of isolation and superior viability [81,82]. However, it is important to note that neonatal cardiomyocytes are more resistant to hypoxia than adult cardiomyocytes, although the mechanisms underlying this resilience are not yet fully understood [83].

In this study, we used the highly sensitive fluorescent biosensor HyPer7 [43] to examine the H_2O_2 levels under oxygen-glucose deprivation conditions. We considered the well-established variations in hypoxic tolerance between adult and neonatal cardiomyocytes, which may correlate with ROS levels during ischemia/reperfusion. We supported hypoxia conditions with glucose deprivation to be closer to *in vivo* conditions of ischemia/reperfusion. We have not observed H_2O_2 production in neonatal cardiomyocytes in contrast to another study, where H_2O_2 production was detected using chemical fluorescent probes in cultured neonatal cardiomyocytes [77]. However, this was observed only after subjecting the cells to a repeated series of hypoxic conditions for 4 days [77]. Our experiments revealed contrasting responses in H_2O_2 levels, illuminating intricate variations in redox signaling and cellular stress within these two developmental stages of cardiomyocytes. Notably, our data demonstrates an elevated concentration of H_2O_2 in adult cardiomyocytes during acute OGD, while in neonatal cardiomyocytes, the H_2O_2 concentration slightly decreased. These findings are consistent with the outcomes observed in our Raman spectroscopy results (Fig. 2) showing the accumulation of electrons in ETC of adult cardiomyocytes under hypoxia, whereas in neonatal cardiomyocytes ETC is fully loaded with electrons under both normoxia and hypoxia conditions indicating almost non-functional ETC state. Besides, by means of RS we have found, that neonatal cardiomyocytes possessed lower total amount of ETC complexes (e.g. mitochondria), than adult cardiomyocytes and that the total amount of ETC complexes in neonatal cells is also lower, than the amount of reduced ETC complexes in adult cells under normoxia. So, neonatal cardiomyocytes cannot generate as much of H_2O_2, as adult cells. We also observed the difference in the cytochrome *c* heme conformation in adult and neonatal cardiomyocytes: in neonatal cells heme of cytochrome *c* has more ruffled conformation that deteriorate processes of the electron acceptance and donation and decreases the rate of electron transport between complexes III and IV.

It's intriguing to note that the differences in hypoxia resistance are closely linked to the distinguishing metabolic characteristics of neonatal and adult cardiomyocytes. These metabolic distinctions undergo significant changes during cardiac development. In the fetal and early postnatal stages of cardiac development, glucose serves as the primary energy substrate, with glycolysis playing a pivotal role in energy production [84–86]. Neonatal hearts predominantly rely on glycolysis for ATP generation, while the rates of fatty acid oxidation remain low. As maturation progresses, there is an increase in fatty acid oxidation rates and an enhanced capacity for glucose oxidation [84,85,87]. Consequently, adult cardiomyocytes heavily depend on continuous mitochondrial activity for ATP production. This is also supported by increased mitochondrial content and the expression of mitochondrial proteins in adult heart compared to neonatal, as was shown by others [85,88] and in our present experiments with Raman microspectroscopy. Additionally, neonatal cardiomyocytes may utilize glycogen accumulated during the fetal period [89] when glucose is insufficient to maintain ATP production. Furthermore, it was indicated that mitochondria may play a role in the mechanism of neonatal hypoxia tolerance, as the mitochondrial permeability transition pore in neonates exhibits lower sensitivity to factors that induce pore opening, such as calcium (Ca^{2+}) [90]. Calcium levels increase during hypoxia due to the enhanced activity of the sodium-calcium exchanger. The reduced mitochondrial quantity and complexity, along with a prevalence of anaerobic glycolysis and elevated glycogen reserves in neonatal cardiomyocytes, may explain the lower levels of H_2O_2 observed during OGD in our study.

Meanwhile, unlike H_2O_2 dynamics, we did not observe significant differences in SypHer3s biosensor responses during OGD/OGR between neonatal and adult cardiomyocytes. Consistent with our previous studies on neurons, the signal from the SypHer3s biosensor decreased significantly, but subsequent OGR restored pH to its initial level [47,91]. This suggests a potentially shared regulation mechanism for pH homeostasis, despite differences in H_2O_2 dynamics, between these cellular stages. It can be explained by more general mechanisms of acidosis development. For example, limited oxygen conditions may lead to a shift from mitochondrial oxidative phosphorylation to anaerobic glycolysis, initiating the accumulation of lactate and an increase in intracellular proton levels [87]. Considering this, our study also delved into the role of acidic metabolite accumulation during cardiac ischemia, which contributes to tissue acidosis. Recognizing the established effect of ischemia on inducing substantial pH changes, this study was designed to investigate the extent of intracellular pH dynamics between neonatal and adult cardiomyocytes using the genetically encoded fluorescent biosensor SypHer3s [44].

The absence of oxygen and nutrient supply triggers an accelerated conversion of pyruvate to lactate via lactate dehydrogenase, along with the regeneration of NAD^+ from NADH, as a mechanism to sustain

anaerobic glycolysis. While glycolysis can indeed generate a limited amount of ATP under ischemic conditions, the hydrolysis of glycolytically derived ATP, in the absence of subsequent pyruvate oxidation, leads to the accumulation of lactate and H^+ in both adult and neonatal cardiomyocytes [87].

Moreover, the rapid restoration of pH equilibrium during subsequent reperfusion can be explained by the mechanisms involving the coordinated action of lactate elimination and activation of the Na^+/H^+ exchanger (NHE) [92] and the Na^+/HCO_3^- symporter [93]. Intracellular proton accumulation during ischemia triggers NHE, which expels protons in exchange for Na^+ entry [92]. Notably, it was shown that NHE expression is rapidly increased in response to ischemia/reperfusion as well as in response to ischemic metabolites such as hydrogen peroxide [94]. The decrease in Na^+/K^+ ATPase activity due to ATP depletion leads to intracellular Na^+ overload, driving the Na^+/Ca^{2+} ion exchanger (NCX) into reverse mode. This, in turn, causes Ca^{2+} overload in both intracellular and mitochondrial compartments, exacerbating damage of the cell [95].

Furthermore, increased ROS production during hypoxia triggers adaptive responses in gene expression that result in the altered biochemical profile of the cell that helps to overcome oxidative stress [96]. In the present study we evaluated the content of cardiac troponin I, troponin T, myoglobin, and GAPDH in neonatal and adult cardiomyocyte cultures under normoxic and hypoxic conditions. All proteins we analyzed are reported to play key roles in different aspects of cell function and metabolism. Troponins I and T are involved in cardiac muscle contraction regulation, myoglobin serves as storage for oxygen in cardiac muscle and GAPDH is a pivotal enzyme in glycolysis. It should be stressed out that neonatal cardiomyocytes might express also slow skeletal isoform of troponin I [97] that displays homology with cardiac isoform up to 52 %. Therefore, to avoid any unspecific detection we measured troponin I cardiac isoform content in cardiomyocytes using sandwich type FIA utilizing monoclonal antibodies 19C7 and 560 that recognizes only cardiac isoform of troponin I. In a normoxic state, adult cardiomyocytes were found to have considerably more analyzed proteins than neonatal cardiomyocytes which is consistent with early findings [98]. It can be explained by the adult cardiomyocytes' more complex contractile apparatus structure, improved contractile function as well as increased metabolic needs. However, under hypoxia neonatal and adult cardiomyocytes displayed different profiles of analyzed proteins. In neonatal cardiomyocytes hypoxia had no effect on the level of measured proteins. This goes along with previously reported suggestions that physiology and metabolism of neonatal cardiomyocytes are resistant to oxygen deficiency conditions. In adult cardiomyocytes under hypoxia troponin T, myoglobin and GAPDH levels were elevated that is consistent with the data that hypoxia promotes cardiac troponin T expression in chicken embryonic heart and adipose-derived adherent stromal cells (ADASs) [30,99] and facilitates GAPDH levels increase in different types of cells [100–102]. It was also demonstrated that not only mRNA and protein content, but also GAPDH enzyme activity increased under hypoxic conditions. For instance, GAPDH enzymatic activity was elevated by 45 % in hypoxic cell homogenates of rat alveolar epithelial cells in the publication of Escoubet et al. [103]. Furthermore, we propose that myoglobin, troponin T, and GAPDH augmentations under hypoxia may indicate important roles in the adaptation of cells to low oxygen levels.

Taken together, these findings support earlier theories suggesting that neonatal hearts are capable of maintaining metabolic and structural homeostasis under hypoxic stress and modified redox state conditions, in contrast to adult ones [104]. This phenomenon is rooted in a fundamental biological process, as fetal hearts evolve under low oxygen availability and subsequently undergo labor-related stress. Consequently, the metabolism of neonatal cardiomyocytes is pre-adapted to oxygen deprivation, enhancing their resilience. Acknowledging this limitation is important during studying redox signaling and metabolism of cardiomyocytes in various cardiovascular pathologies.

5. Author disclosure statement

No competing financial interests exist.

Declaration of competing interest

The authors declare that they have no known competing financial interests or personal relationships that could have appeared to influence the work reported in this paper.

Acknowledgements

This research has been supported by the Interdisciplinary Scientific and Educational School of Moscow University «Molecular Technologies of the Living Systems and Synthetic Biology» grant 23-III04-48.

References

[1] The top 10 causes of death, n.d. https://www.who.int/news-room/fact-sheets/detail/the-top-10-causes-of-death. (Accessed 28 September 2023).
[2] G.A. Roth, G.A. Mensah, et al., Global burden of cardiovascular diseases and risk factors, 1990–2019: update from the GBD 2019 study, J. Am. Coll. Cardiol. 76 (2020) 2982–3021, https://doi.org/10.1016/j.jacc.2020.11.010.
[3] F.J. Giordano, Oxygen, oxidative stress, hypoxia, and heart failure, J. Clin. Invest. 115 (2005) 500–508, https://doi.org/10.1172/JCI24408.
[4] M. Seddon, Y.H. Looi, A.M. Shah, Oxidative stress and redox signalling in cardiac hypertrophy and heart failure, Heart 93 (2007) 903–907, https://doi.org/10.1136/hrt.2005.068270.
[5] D. Moris, M. Spartalis, E. Spartalis, G.-S. Karachaliou, G.I. Karaolanis, G. Tsourouflis, D.I. Tsilimigras, E. Tzatzaki, S. Theocharis, The role of reactive oxygen species in the pathophysiology of cardiovascular diseases and the clinical significance of myocardial redox, Ann. Transl. Med. 5 (2017), https://doi.org/10.21037/atm.2017.06.27, 326–326.
[6] Q. Xu, A. Dalic, L. Fang, H. Kiriazis, R. Ritchie, K. Sim, X.-M. Gao, G. Drummond, M. Sarwar, Y.-Y. Zhang, A. Dart, X.-J. Du, Myocardial oxidative stress contributes to transgenic β2-adrenoceptor activation-induced cardiomyopathy and heart failure, Br. J. Pharmacol. 162 (2011) 1012–1028, https://doi.org/10.1111/j.1476-5381.2010.01043.x.
[7] J.R. Burgoyne, H. Mongue-Din, P. Eaton, A.M. Shah, Redox signaling in cardiac physiology and pathology, Circ. Res. 111 (2012) 1091–1106, https://doi.org/10.1161/CIRCRESAHA.111.255216.
[8] D.I. Brown, K.K. Griendling, Regulation of signal transduction by reactive oxygen species in the cardiovascular system, Circ. Res. 116 (2015) 531–549, https://doi.org/10.1161/CIRCRESAHA.116.303584.
[9] J. Nordberg, E.S.J. Arnér, Reactive oxygen species, antioxidants, and the mammalian thioredoxin system, Free Radic. Biol. Med. 31 (2001) 1287–1312, https://doi.org/10.1016/S0891-5849(01)00724-9.
[10] B. Halliwell, Drug antioxidant effects, Drugs 42 (1991) 569–605, https://doi.org/10.2165/00003495-199142040-00003.
[11] R. Brigelius-Flohé, K. Wingler, C. Müller, [9] - estimation of individual types of glutathione peroxidases, in: H. Sies, L. Packer (Eds.), Methods Enzymol., Academic Press, 2002, pp. 101–112, https://doi.org/10.1016/S0076-6879(02)47011-5.
[12] R. Brigelius-Flohé, Tissue-specific functions of individual glutathione peroxidases, Free Radic. Biol. Med. 27 (1999) 951–965, https://doi.org/10.1016/S0891-5849(99)00173-2.
[13] T. Finkel, Signal transduction by reactive oxygen species, J. Cell Biol. 194 (2011) 7–15, https://doi.org/10.1083/jcb.201102095.
[14] W. Dröge, Free radicals in the physiological control of cell function, Physiol. Rev. 82 (2002) 47–95, https://doi.org/10.1152/physrev.00018.2001.
[15] H. Sies, Hydrogen peroxide as a central redox signaling molecule in physiological oxidative stress: oxidative eustress, Redox Biol. 11 (2017) 613–619, https://doi.org/10.1016/j.redox.2016.12.035.
[16] J. Liang, M. Wu, C. Chen, M. Mai, J. Huang, P. Zhu, Roles of reactive oxygen species in cardiac differentiation, reprogramming, and regenerative therapies, Oxid. Med. Cell. Longev. 2020 (2020), e2102841, https://doi.org/10.1155/2020/2102841.
[17] R. D'Oria, R. Schipani, A. Leonardini, A. Natalicchio, S. Perrini, A. Cignarelli, L. Laviola, F. Giorgino, The role of oxidative stress in cardiac disease: from physiological response to injury factor, Oxid. Med. Cell. Longev. 2020 (2020), e5732956, https://doi.org/10.1155/2020/5732956.
[18] A.V. Zima, L.A. Blatter, Redox regulation of cardiac calcium channels and transporters, Cardiovasc. Res. 71 (2006) 310–321, https://doi.org/10.1016/j.cardiores.2006.02.019.
[19] P. Venditti, P. Masullo, S. Di Meo, Effects of myocardial ischemia and reperfusion on mitochondrial function and susceptibility to oxidative stress, Cell. Mol. Life Sci. CMLS. 58 (2001) 1528–1537, https://doi.org/10.1007/PL00000793.
[20] P. Venditti, R. De Rosa, L. Cigliano, C. Agnisola, S. Di Meo, Role of nitric oxide in the functional response to ischemia-reperfusion of heart mitochondria from hyperthyroid rats, Cell. Mol. Life Sci. CMLS. 61 (2004) 2244–2252, https://doi.org/10.1007/s00018-004-4125-9.

[21] D.J. Hausenloy, D.M. Yellon, Myocardial ischemia-reperfusion injury: a neglected therapeutic target, J. Clin. Invest. 123 (2013) 92–100, https://doi.org/10.1172/JCI62874.
[22] S. Cadenas, J. Aragonés, M.O. Landázuri, Mitochondrial reprogramming through cardiac oxygen sensors in ischaemic heart disease, Cardiovasc. Res. 88 (2010) 219–228, https://doi.org/10.1093/cvr/cvq256.
[23] E.J. Benjamin, P. Muntner, A. Alonso, M.S. Bittencourt, C.W. Callaway, A. P. Carson, A.M. Chamberlain, A.R. Chang, S. Cheng, S.R. Das, F.N. Delling, L. Djousse, M.S.V. Elkind, J.F. Ferguson, M. Fornage, L.C. Jordan, S.S. Khan, B. M. Kissela, K.L. Knutson, T.W. Kwan, D.T. Lackland, T.T. Lewis, J.H. Lichtman, C. T. Longenecker, M.S. Loop, P.L. Lutsey, S.S. Martin, K. Matsushita, A.E. Moran, M. E. Mussolino, M. O'Flaherty, A. Pandey, A.M. Perak, W.D. Rosamond, G.A. Roth, U.K.A. Sampson, G.M. Satou, E.B. Schroeder, S.H. Shah, N.L. Spartano, A. Stokes, D.L. Tirschwell, C.W. Tsao, M.P. Turakhia, L.B. VanWagner, J.T. Wilkins, S. S. Wong, S.S. Virani, American heart association council on epidemiology and prevention statistics committee and stroke statistics subcommittee, heart disease and stroke statistics-2019 update: a report from the American heart association, Circulation 139 (2019), e56, https://doi.org/10.1161/CIR.0000000000000659 e528.
[24] E.T. Chouchani, V.R. Pell, A.M. James, L.M. Work, K. Saeb-Parsy, C. Frezza, T. Krieg, M.P. Murphy, A unifying mechanism for mitochondrial superoxide production during ischemia-reperfusion injury, Cell Metab 23 (2016) 254–263, https://doi.org/10.1016/j.cmet.2015.12.009.
[25] E.T. Chouchani, V.R. Pell, E. Gaude, D. Aksentijević, S.Y. Sundier, E.L. Robb, A. Logan, S.M. Nadtochiy, E.N.J. Ord, A.C. Smith, F. Eyassu, R. Shirley, C.-H. Hu, A.J. Dare, A.M. James, S. Rogatti, R.C. Hartley, S. Eaton, A.S.H. Costa, P. S. Brookes, S.M. Davidson, M.R. Duchen, K. Saeb-Parsy, M.J. Shattock, A. J. Robinson, L.M. Work, C. Frezza, T. Krieg, M.P. Murphy, Ischaemic accumulation of succinate controls reperfusion injury through mitochondrial ROS, Nature 515 (2014) 431–435, https://doi.org/10.1038/nature13909.
[26] T. Zhou, C.-C. Chuang, L. Zuo, Molecular characterization of reactive oxygen species in myocardial ischemia-reperfusion injury, BioMed Res. Int. 2015 (2015), e864946, https://doi.org/10.1155/2015/864946.
[27] L. Zuo, T. Zhou, B.K. Pannell, A.C. Ziegler, T.M. Best, Biological and physiological role of reactive oxygen species – the good, the bad and the ugly, Acta Physiol. 214 (2015) 329–348, https://doi.org/10.1111/apha.12515.
[28] X. Zhu, L. Zuo, Characterization of oxygen radical formation mechanism at early cardiac ischemia, Cell Death Dis. 4 (2013), e787, https://doi.org/10.1038/cddis.2013.313 e787.
[29] D.N. Granger, P.R. Kvietys, Reperfusion injury and reactive oxygen species: the evolution of a concept, Redox Biol. 6 (2015) 524–551, https://doi.org/10.1016/j.redox.2015.08.020.
[30] S. Druyan, A. Cahaner, C.M. Ashwell, The expression patterns of hypoxia-inducing factor subunit α-1, heme oxygenase, hypoxia upregulated protein 1, and cardiac troponin T during development of the chicken heart, Poult. Sci. 86 (2007) 2384–2389, https://doi.org/10.3382/ps.2007-00152.
[31] I.-C. Lee, C.-S. Yu, S.-H. Wong, K.-H. Lue, Troponin I levels in neonatal hypoxic–ischemic encephalopathy are related to cardiopulmonary comorbidity and neurodevelopmental outcomes, J. Clin. Med. 10 (2021) 4010, https://doi.org/10.3390/jcm10174010.
[32] J. Fraser, L. Vieira de Mello, D. Ward, H.H. Rees, D.R. Williams, Y. Fang, A. Brass, A.Y. Gracey, A.R. Cossins, Hypoxia-inducible myoglobin expression in nonmuscle tissues, Proc. Natl. Acad. Sci. 103 (2006) 2977–2981, https://doi.org/10.1073/pnas.0508270103.
[33] V.V. Belousov, A.F. Fradkov, K.A. Lukyanov, D.B. Staroverov, K.S. Shakhbazov, A. V. Terskikh, S. Lukyanov, Genetically encoded fluorescent indicator for intracellular hydrogen peroxide, Nat. Methods 3 (2006) 281–286, https://doi.org/10.1038/nmeth866.
[34] P. Niethammer, C. Grabher, A.T. Look, T.J. Mitchison, A tissue-scale gradient of hydrogen peroxide mediates rapid wound detection in zebrafish, Nature 459 (2009) 996–999, https://doi.org/10.1038/nature08119.
[35] L. Pase, J.E. Layton, C. Wittmann, F. Ellett, C.J. Nowell, C.C. Reyes-Aldasoro, S. Varma, K.L. Rogers, C.J. Hall, M.C. Keightley, P.S. Crosier, C. Grabher, J. K. Heath, S.A. Renshaw, G.J. Lieschke, Neutrophil-delivered myeloperoxidase dampens the hydrogen peroxide burst after tissue Wounding in zebrafish, Curr. Biol. 22 (2012) 1818–1824, https://doi.org/10.1016/j.cub.2012.07.060.
[36] P. Back, W.H. De Vos, G.G. Depuydt, F. Matthijssens, J.R. Vanfleteren, B. P. Braeckman, Exploring real-time in vivo redox biology of developing and aging Caenorhabditis elegans, Free Radic. Biol. Med. 52 (2012) 850–859, https://doi.org/10.1016/j.freeradbiomed.2011.11.037.
[37] D.S. Bilan, V.V. Belousov, HyPer family probes: state of the Art, Antioxid. Redox Signal. 24 (2016) 731–751, https://doi.org/10.1089/ars.2015.6586.
[38] T. Yoshida, S. Alfaqaan, N. Sasaoka, H. Imamura, Application of FRET-based biosensor "ATeam" for visualization of ATP levels in the mitochondrial matrix of living mammalian cells, in: D. Mokranjac, F. Perocchi (Eds.), Mitochondria Pract. Protoc., Springer, New York, NY, 2017, pp. 231–243, https://doi.org/10.1007/978-1-4939-6824-4_14.
[39] K. Harada, T. Chihara, Y. Hayasaka, M. Mita, M. Takizawa, K. Ishida, M. Arai, S. Tsuno, M. Matsumoto, T. Ishihara, H. Ueda, T. Kitaguchi, T. Tsuboi, Green fluorescent protein-based lactate and pyruvate indicators suitable for biochemical assays and live cell imaging, Sci. Rep. 10 (2020), 19562, https://doi.org/10.1038/s41598-020-76440-4.
[40] C.L. Miller, Y. Cai, M. Oikawa, T. Thomas, W.R. Dostmann, M. Zaccolo, K. Fujiwara, C. Yan, Cyclic nucleotide phosphodiesterase 1A: a key regulator of cardiac fibroblast activation and extracellular matrix remodeling in the heart, Basic Res. Cardiol. 106 (2011) 1023–1039, https://doi.org/10.1007/s00395-011-0228-2.
[41] G. Calamera, D. Li, A.H. Ulsund, J.J. Kim, O.C. Neely, L.R. Moltzau, M. Bjørnerem, D. Paterson, C. Kim, F.O. Levy, K.W. Andressen, FRET-based cyclic GMP biosensors measure low cGMP concentrations in cardiomyocytes and neurons, Commun. Biol. 2 (2019) 1–12, https://doi.org/10.1038/s42003-019-0641-x.
[42] O. Lomas, M. Brescia, R. Carnicer, S. Monterisi, N.C. Surdo, M. Zaccolo, Adenoviral transduction of FRET-based biosensors for cAMP in primary adult mouse cardiomyocytes, in: M. Zaccolo (Ed.), CAMP Signal. Methods Protoc., Springer, New York, NY, 2015, pp. 103–115, https://doi.org/10.1007/978-1-4939-2537-7_8.
[43] V.V. Pak, D. Ezeriņa, O.G. Lyublinskaya, B. Pedre, P.A. Tyurin-Kuzmin, N. M. Mishina, M. Thauvin, D. Young, K. Wahni, S.A.M. Gache, A.D. Demidovich, Y. G. Ermakova, Y.D. Maslova, A.G. Shokhina, E. Eroglu, D.S. Bilan, I. Bogeski, T. Michel, S. Vriz, J. Messens, V.V. Belousov, Ultrasensitive genetically encoded indicator for hydrogen peroxide identifies roles for the oxidant in cell migration and mitochondrial function, Cell Metab 31 (2020) 642–653.e6, https://doi.org/10.1016/j.cmet.2020.02.003.
[44] Y.G. Ermakova, V.V. Pak, Y.A. Bogdanova, A.A. Kotlobay, I.V. Yampolsky, A. G. Shokhina, A.S. Panova, R.A. Marygin, D.B. Staroverov, D.S. Bilan, H. Sies, V. V. Belousov, SypHer3s: a genetically encoded fluorescent ratiometric probe with enhanced brightness and an improved dynamic range, Chem. Commun. 54 (2018) 2898–2901, https://doi.org/10.1039/C7CC08740C.
[45] P. Alam, B.D. Maliken, M.J. Ivey, S.M. Jones, O. Kanisicak, Isolation, transfection, and long-term culture of adult mouse and rat cardiomyocytes, JoVE J. Vis. Exp. (2020), e61073, https://doi.org/10.3791/61073.
[46] R. Rizzuto, H. Nakase, B. Darras, U. Francke, G.M. Fabrizi, T. Mengel, F. Walsh, B. Kadenbach, S. DiMauro, E.A. Schon, A gene specifying subunit VIII of human cytochrome c oxidase is localized to chromosome 11 and is expressed in both muscle and non-muscle tissues, J. Biol. Chem. 264 (1989) 10595–10600, https://doi.org/10.1016/S0021-9258(18)81662-3.
[47] I.V. Kelmanson, A.G. Shokhina, D.A. Kotova, M.S. Pochechuev, A.D. Ivanova, A. I. Kostyuk, A.S. Panova, A.A. Borodinova, M.A. Solotenkov, E.A. Stepanov, R. I. Raevskii, A.A. Moshchenko, V.V. Pak, Y.G. Ermakova, G.J.C. van Belle, V. Tarabykin, P.M. Balaban, I.V. Fedotov, A.B. Fedotov, M. Conrad, I. Bogeski, D. M. Katschinski, T.R. Doeppner, M. Bähr, A.M. Zheltikov, V.V. Belousov, D. S. Bilan, In vivo dynamics of acidosis and oxidative stress in the acute phase of an ischemic stroke in a rodent model, Redox Biol. 48 (2021), 102178, https://doi.org/10.1016/j.redox.2021.102178.
[48] I.A. Katrukha, N.S. Riabkova, A.E. Kogan, A.V. Vylegzhanina, K. Sh Mukharyamova, A.P. Bogomolova, A.I. Zabolotskii, E.V. Koshkina, A. V. Bereznikova, A.G. Katrukha, Fragmentation of human cardiac troponin T after acute myocardial infarction, Clin. Chim. Acta 542 (2023), 117281, https://doi.org/10.1016/j.cca.2023.117281.
[49] M.M. Bradford, A rapid and sensitive method for the quantitation of microgram quantities of protein utilizing the principle of protein-dye binding, Anal. Biochem. 72 (1976) 248–254, https://doi.org/10.1016/0003-2697(76)90527-3.
[50] H. Towbin, T. Staehelin, J. Gordon, Electrophoretic transfer of proteins from polyacrylamide gels to nitrocellulose sheets: procedure and some applications, Proc. Natl. Acad. Sci. 76 (1979) 4350–4354, https://doi.org/10.1073/pnas.76.9.4350.
[51] Y. Sun, A. Benabbas, W. Zeng, J.G. Kleingardner, K.L. Bren, P.M. Champion, Investigations of heme distortion, low-frequency vibrational excitations, and electron transfer in cytochrome c, Proc. Natl. Acad. Sci. 111 (2014) 6570–6575, https://doi.org/10.1073/pnas.1322274111.
[52] P. Bazylewski, R. Divigalpitiya, G. Fanchini, In situ Raman spectroscopy distinguishes between reversible and irreversible thiol modifications in L-cysteine, RSC Adv. 7 (2017) 2964–2970, https://doi.org/10.1039/C6RA25879D.
[53] N.A. Brazhe, M. Treiman, A.R. Brazhe, N.L. Find, G.V. Maksimov, O. V. Sosnovtseva, Mapping of redox state of mitochondrial cytochromes in live cardiomyocytes using Raman microspectroscopy, PLoS One 7 (2012), e41990, https://doi.org/10.1371/journal.pone.0041990.
[54] N.A. Brazhe, M. Treiman, B. Faricelli, J.H. Vestergaard, O. Sosnovtseva, In situ Raman study of redox state changes of mitochondrial cytochromes in a perfused rat heart, PLoS One 8 (2013), e70488, https://doi.org/10.1371/journal.pone.0070488.
[55] T. Yamamoto, T. Minamikawa, Y. Harada, Y. Yamaoka, H. Tanaka, H. Yaku, T. Takamatsu, Label-free evaluation of myocardial infarct in surgically excised ventricular myocardium by Raman spectroscopy, Sci. Rep. 8 (2018), 14671, https://doi.org/10.1038/s41598-018-33025-6.
[56] D.T. Love, C. Guo, E.I. Nikelshparg, N.A. Brazhe, O. Sosnovtseva, C.L. Hawkins, The role of the myeloperoxidase-derived oxidant hypothiocyanous acid (HOSCN) in the induction of mitochondrial dysfunction in macrophages, Redox Biol. 36 (2020), 101602, https://doi.org/10.1016/j.redox.2020.101602.
[57] M. Okada, N.I. Smith, A.F. Palonpon, H. Endo, S. Kawata, M. Sodeoka, K. Fujita, Label-free Raman observation of cytochrome c dynamics during apoptosis, Proc. Natl. Acad. Sci. 109 (2012) 28–32, https://doi.org/10.1073/pnas.1107524108.
[58] M. Ogawa, Y. Harada, Y. Yamaoka, K. Fujita, H. Yaku, T. Takamatsu, Label-free biochemical imaging of heart tissue with high-speed spontaneous Raman microscopy, Biochem. Biophys. Res. Commun. 382 (2009) 370–374, https://doi.org/10.1016/j.bbrc.2009.03.028.
[59] A. Popov, N. Brazhe, A. Fedotova, A. Tiaglik, M. Bychkov, K. Morozova, A. Brazhe, D. Aronov, E. Lyukmanova, N. Lazareva, L. Li, E. Ponimaskin, A. Verkhratsky, A. Semyanov, A high-fat diet changes astrocytic metabolism to

promote synaptic plasticity and behavior, Acta Physiol. 236 (2022), e13847, https://doi.org/10.1111/apha.13847.
[60] C.-M. Moon, Y.-H. Kim, Y.-K. Ahn, M.-H. Jeong, G.-W. Jeong, Metabolic alterations in acute myocardial ischemia-reperfusion injury and necrosis using in vivo hyperpolarized [1-13C] pyruvate MR spectroscopy, Sci. Rep. 9 (2019), 18427, https://doi.org/10.1038/s41598-019-54965-7.
[61] J. Inserte, D. Aluja, I. Barba, M. Ruiz-Meana, E. Miró, M. Poncelas, Ú. Vilardosa, J. Castellano, D. Garcia-Dorado, High-fat diet improves tolerance to myocardial ischemia by delaying normalization of intracellular PH at reperfusion, J. Mol. Cell. Cardiol. 133 (2019) 164–173, https://doi.org/10.1016/j.yjmcc.2019.06.001.
[62] Y. Sun, V. Karunakaran, P.M. Champion, Investigations of the low-frequency spectral density of cytochrome c upon equilibrium unfolding, J. Phys. Chem. B 117 (2013) 9615–9625, https://doi.org/10.1021/jp404881k.
[63] R.V. Chertkova, N.A. Brazhe, T.V. Bryantseva, A.N. Nekrasov, D.A. Dolgikh, A. I. Yusipovich, O. Sosnovtseva, G.V. Maksimov, A.B. Rubin, M.P. Kirpichnikov, New insight into the mechanism of mitochondrial cytochrome c function, PLoS One 12 (2017), e0178280, https://doi.org/10.1371/journal.pone.0178280.
[64] T. Presley, K. Vedam, X. Liu, J.L. Zweier, G. Ilangovan, Activation of Hsp90/NOS and increased NO generation does not impair mitochondrial respiratory chain by competitive binding at cytochrome C Oxidase in low oxygen concentrations, Cell Stress Chaperones 14 (2009) 611–627, https://doi.org/10.1007/s12192-009-0114-0.
[65] C.T. Taylor, S. Moncada, Nitric oxide, cytochrome C oxidase, and the cellular response to hypoxia, Arterioscler. Thromb. Vasc. Biol. 30 (2010) 643–647, https://doi.org/10.1161/ATVBAHA.108.181628.
[66] C. Gu, S. Park, J. Seok, H.Y. Jang, Y.J. Bang, G.I.J. Kim, Altered expression of ADM and ADM2 by hypoxia regulates migration of trophoblast and HLA-G expression, Biol. Reprod. 104 (2021) 159–169, https://doi.org/10.1093/biolre/ioaa178.
[67] J. Korbecki, K. Kojder, K. Barczak, D. Simińska, I. Gutowska, D. Chlubek, I. Baranowska-Bosiacka, Hypoxia alters the expression of CC chemokines and CC chemokine receptors in a tumor–A literature review, Int. J. Mol. Sci. 21 (2020) 5647, https://doi.org/10.3390/ijms21165647.
[68] Z. Luo, M. Tian, G. Yang, Q. Tan, Y. Chen, G. Li, Q. Zhang, Y. Li, P. Wan, J. Wu, Hypoxia signaling in human health and diseases: implications and prospects for therapeutics, Signal Transduct. Target. Ther. 7 (2022) 1–30, https://doi.org/10.1038/s41392-022-01080-1.
[69] V. Lauer, S. Grampp, J. Platt, V. Lafleur, O. Lombardi, H. Choudhry, F. Kranz, A. Hartmann, B. Wullich, A. Yamamoto, M.L. Coleman, P.J. Ratcliffe, D.R. Mole, J. Schödel, Hypoxia drives glucose transporter 3 expression through hypoxia-inducible transcription factor (HIF)-mediated induction of the long noncoding RNA NICI, J. Biol. Chem. 295 (2020) 4065–4078, https://doi.org/10.1074/jbc.RA119.009827.
[70] C.J.A. Ramachandra, S. Hernandez-Resendiz, G.E. Crespo-Avilan, Y.-H. Lin, D. J. Hausenloy, Mitochondria in acute myocardial infarction and cardioprotection, EBioMedicine 57 (2020), 102884, https://doi.org/10.1016/j.ebiom.2020.102884.
[71] F.G. Akar, M.A. Aon, G.F. Tomaselli, B. O'Rourke, The mitochondrial origin of postischemic arrhythmias, J. Clin. Invest. 115 (2005) 3527–3535, https://doi.org/10.1172/JCI25371.
[72] S. Matsushima, H. Tsutsui, J. Sadoshima, Physiological and pathological functions of NADPH oxidases during myocardial ischemia–reperfusion, Trends Cardiovasc. Med. 24 (2014) 202–205, https://doi.org/10.1016/j.tcm.2014.03.003.
[73] S.-G. Ong, W.H. Lee, L. Theodorou, K. Kodo, S.Y. Lim, D.H. Shukla, T. Briston, S. Kiriakidis, M. Ashcroft, S.M. Davidson, P.H. Maxwell, D.M. Yellon, D. J. Hausenloy, HIF-1 reduces ischaemia-reperfusion injury in the heart by targeting the mitochondrial permeability transition pore, Cardiovasc. Res. 104 (2014) 24–36, https://doi.org/10.1093/cvr/cvu172.
[74] S. Hamilton, R. Terentyeva, T.Y. Kim, P. Bronk, R.T. Clements, J. O-Uchi, G. Csordás, B.-R. Choi, D. Terentyev, Pharmacological modulation of mitochondrial Ca2+ content regulates sarcoplasmic reticulum Ca2+ release via oxidation of the ryanodine receptor by mitochondria-derived reactive oxygen species, Front. Physiol. 9 (2018). https://www.frontiersin.org/articles/10.3389/fphys.2018.01831. (Accessed 28 September 2023).
[75] B. Steinhorn, A. Sorrentino, S. Badole, Y. Bogdanova, V. Belousov, T. Michel, Chemogenetic generation of hydrogen peroxide in the heart induces severe cardiac dysfunction, Nat. Commun. 9 (2018) 4044, https://doi.org/10.1038/s41467-018-06533-2.
[76] M.L. Lindsey, R. Bolli, J.M. Canty, X.-J. Du, N.G. Frangogiannis, S. Frantz, R. G. Gourdie, J.W. Holmes, S.P. Jones, R.A. Kloner, D.J. Lefer, R. Liao, E. Murphy, P. Ping, K. Przyklenk, F.A. Recchia, L. Schwartz Longacre, C.M. Ripplinger, J. E. Van Eyk, G. Heusch, Guidelines for experimental models of myocardial ischemia and infarction, Am. J. Physiol. Heart Circ. Physiol. 314 (2018) H812–H838, https://doi.org/10.1152/ajpheart.00335.2017.
[77] S.G. Canfield, A. Sepac, F. Sedlic, M.Y. Muravyeva, X. Bai, Z.J. Bosnjak, Marked hyperglycemia attenuates anesthetic preconditioning in human-induced pluripotent stem cell-derived cardiomyocytes, Anesthesiology 117 (2012) 735–744, https://doi.org/10.1097/ALN.0b013e3182655e96.
[78] L. Portal, V. Martin, R. Assaly, A. d'Anglemont de Tassigny, S. Michineau, A. Berdeaux, B. Ghaleb, S. Pons, A model of hypoxia-reoxygenation on isolated adult mouse cardiomyocytes: characterization, comparison with ischemia-reperfusion, and application to the cardioprotective effect of regular treadmill exercise, J. Cardiovasc. Pharmacol. Ther. 18 (2013) 367–375, https://doi.org/10.1177/1074248412475158.
[79] M.P. Mori, R. Penjweini, J.R. Knutson, P. Wang, P.M. Hwang, Mitochondria and oxygen homeostasis, FEBS J. 289 (2022) 6959–6968, https://doi.org/10.1111/febs.16115.
[80] M.S. Nanadikar, A.M. Vergel Leon, S. Borowik, A. Hillemann, A. Zieseniss, V. V. Belousov, I. Bogeski, P. Rehling, J. Dudek, D.M. Katschinski, O2 affects mitochondrial functionality ex vivo, Redox Biol. 22 (2019), 101152, https://doi.org/10.1016/j.redox.2019.101152.
[81] H.-R. Chang, C.-F. Lien, J.-R. Jeng, J.-C. Hsieh, C.-W. Chang, J.-H. Lin, K.-T. Yang, Intermittent hypoxia inhibits Na+-H+ exchange-mediated acid extrusion via intracellular Na+ accumulation in cardiomyocytes, Cell. Physiol. Biochem. Int. J. Exp. Cell. Physiol. Biochem. Pharmacol. 46 (2018) 1252–1262, https://doi.org/10.1159/000489076.
[82] J.-C. Fernández-Morales, M. Morad, Regulation of Ca2+ signaling by acute hypoxia and acidosis in rat neonatal cardiomyocytes, J. Mol. Cell. Cardiol. 114 (2018) 58–71, https://doi.org/10.1016/j.yjmcc.2017.10.004.
[83] I. Ostadalova, B. Ostadal, F. Kolář, J.R. Parratt, S. Wilson, Tolerance to ischaemia and ischaemic preconditioning in neonatal rat heart, J. Mol. Cell. Cardiol. 30 (1998) 857–865, https://doi.org/10.1006/jmcc.1998.0653.
[84] J. Girard, P. Ferre, J.P. Pegorier, P.H. Duee, Adaptations of glucose and fatty acid metabolism during perinatal period and suckling-weaning transition, Physiol. Rev. 72 (1992) 507–562, https://doi.org/10.1152/physrev.1992.72.2.507.
[85] J. Piquereau, R. Ventura-Clapier, Maturation of cardiac energy metabolism during perinatal development, Front. Physiol. 9 (2018). https://www.frontiersin.org/articles/10.3389/fphys.2018.00959. (Accessed 28 September 2023).
[86] G.D. Lopaschuk, M.A. Spafford, D.R. Marsh, Glycolysis is predominant source of myocardial ATP production immediately after birth, Am. J. Physiol. Heart Circ. Physiol. 261 (1991) H1698–H1705, https://doi.org/10.1152/ajpheart.1991.261.6.H1698.
[87] G.D. Lopaschuk, J.R. Ussher, C.D.L. Folmes, J.S. Jaswal, W.C. Stanley, Myocardial fatty acid metabolism in health and disease, Physiol. Rev. 90 (2010) 207–258, https://doi.org/10.1152/physrev.00015.2009.
[88] B.N. Puente, W. Kimura, S.A. Muralidhar, J. Moon, J.F. Amatruda, K.L. Phelps, D. Grinsfelder, B.A. Rothermel, R. Chen, J.A. Garcia, C.X. Santos, S. Thet, E. Mori, M.T. Kinter, P.M. Rindler, S. Zacchigna, S. Mukherjee, D.J. Chen, A.I. Mahmoud, M. Giacca, P.S. Rabinovitch, A. Aroumougame, A.M. Shah, L.I. Szweda, H. A. Sadek, The oxygen-rich postnatal environment induces cardiomyocyte cell-cycle arrest through DNA damage response, Cell 157 (2014) 565–579, https://doi.org/10.1016/j.cell.2014.03.032.
[89] T.M.A. Mohamed, R. Abouleisa, B.G. Hill, Metabolic determinants of cardiomyocyte proliferation, Stem Cells Dayt. Ohio. 40 (2022) 458–467, https://doi.org/10.1093/stmcls/sxac016.
[90] M. Milerova, Z. Charvatova, L. Skarka, I. Ostadalova, Z. Drahota, M. Fialova, B. Ostadal, Neonatal cardiac mitochondria and ischemia/reperfusion injury, Mol. Cell. Biochem. 335 (2010) 147–153, https://doi.org/10.1007/s11010-009-0251-x.
[91] D.A. Kotova, A.D. Ivanova, M.S. Pochechuev, I.V. Kelmanson, Y.V. Khramova, A. Tiaglik, M.A. Sudoplatov, A.P. Trifonova, A. Fedotova, K. Morozova, V. A. Katrukha, A.D. Sergeeva, R.I. Raevskii, M.P. Pestriakova, M.A. Solotenkov, E. A. Stepanov, A.S. Tsopina, A.A. Moshchenko, M. Shestopalova, A. Zalygin, I. V. Fedotov, A.B. Fedotov, V. Oleinikov, V.V. Belousov, A. Semyanov, N. Brazhe, A.M. Zheltikov, D.S. Bilan, Hyperglycemia exacerbates ischemic stroke not through increased generation of hydrogen peroxide, Free Radic. Biol. Med. 208 (2023) 153–164, https://doi.org/10.1016/j.freeradbiomed.2023.08.004.
[92] M. Avkiran, M.S. Marber, Na(+)/H(+) exchange inhibitors for cardioprotective therapy: progress, problems and prospects, J. Am. Coll. Cardiol. 39 (2002) 747–753, https://doi.org/10.1016/s0735-1097(02)01693-5.
[93] M. Lu, M. Jia, Q. Wang, Y. Guo, C. Li, B. Ren, F. Qian, J. Wu, The electrogenic sodium bicarbonate cotransporter and its roles in the myocardial ischemia-reperfusion induced cardiac diseases, Life Sci. 270 (2021), 119153, https://doi.org/10.1016/j.lfs.2021.119153.
[94] X.T. Gan, S. Chakrabarti, M. Karmazyn, Modulation of Na+/H+exchange isoform 1 mRNA expression in isolated rat hearts, Am. J. Physiol. Heart Circ. Physiol. 277 (1999) H993–H998, https://doi.org/10.1152/ajpheart.1999.277.3.H993.
[95] M. Karmazyn, X.T. Gan, R.A. Humphreys, H. Yoshida, K. Kusumoto, The myocardial Na+-H+ exchange, Circ. Res. 85 (1999) 777–786, https://doi.org/10.1161/01.RES.85.9.777.
[96] A.M. Pickering, L. Vojtovich, J. Tower, K.J. A Davies, Oxidative stress adaptation with acute, chronic, and repeated stress, Free Radic. Biol. Med. 55 (2013) 109–118, https://doi.org/10.1016/j.freeradbiomed.2012.11.001.
[97] S. Sasse, N.J. Brand, P. Kyprianou, G.K. Dhoot, R. Wade, M. Arai, M. Periasamy, M.H. Yacoub, P.J. Barton, Troponin I gene expression during human cardiac development and in end-stage heart failure, Circ. Res. 72 (1993) 932–938, https://doi.org/10.1161/01.res.72.5.932.
[98] S.P. Bishop, J. Zhang, L. Ye, Cardiomyocyte proliferation from fetal- to adult- and from normal- to hypertrophy and failing hearts, Biology 11 (2022) 880, https://doi.org/10.3390/biology11060880.
[99] J.-W. Choi, H. Moon, S.E. Jung, S. Lim, S. Lee, I.-K. Kim, H.-B. Lee, J. Lee, B.-W. Song, S.W. Kim, K.-C. Hwang, Hypoxia rapidly induces the expression of cardiomyogenic factors in human adipose-derived adherent stromal cells, J. Clin. Med. 8 (2019) 1231, https://doi.org/10.3390/jcm8081231.
[100] B. Escoubet, C. Planès, C. Clerici, Hypoxia increases glyceraldehyde-3-phosphate dehydrogenase transcription in rat alveolar epithelial cells, Biochem. Biophys. Res. Commun. 266 (1999) 156–161, https://doi.org/10.1006/bbrc.1999.1798.
[101] R. Yamaji, K. Fujita, S. Takahashi, H. Yoneda, K. Nagao, W. Masuda, M. Naito, T. Tsuruo, K. Miyatake, H. Inui, Y. Nakano, Hypoxia up-regulates glyceraldehyde-3-phosphate dehydrogenase in mouse brain capillary endothelial cells:

involvement of Na+/Ca2+ exchanger, Biochim. Biophys. Acta BBA - Mol. Cell Res. 1593 (2003) 269–276, https://doi.org/10.1016/S0167-4889(02)00397-X.
[102] Y. Higashimura, Y. Nakajima, R. Yamaji, N. Harada, F. Shibasaki, Y. Nakano, H. Inui, Up-regulation of glyceraldehyde-3-phosphate dehydrogenase gene expression by HIF-1 activity depending on Sp1 in hypoxic breast cancer cells, Arch. Biochem. Biophys. 509 (2011) 1–8, https://doi.org/10.1016/j.abb.2011.02.011.
[103] B. Escoubet, C. Planès, C. Clerici, Hypoxia increases glyceraldehyde-3-phosphate dehydrogenase transcription in rat alveolar epithelial cells, Biochem. Biophys. Res. Commun. 266 (1999) 156–161, https://doi.org/10.1006/bbrc.1999.1798.
[104] A.J. Patterson, L. Zhang, Hypoxia and fetal heart development, Curr. Mol. Med. 10 (2010) 653–666, https://doi.org/10.2174/156652410792630643.